QUANTUM NOISE IN NONLINEAR OPTICAL PHENOMENA

RYSZARD TANAŚ

Nonlinear Optics Division, Institute of Physics, Adam Mickiewicz University, Poznań, Poland

CONTENTS

I. INTRODUCTION

More than a century has passed since Planck discovered that it is possible to explain properties of the blackbody radiation by introducing discrete packets of energy, which we now call *photons*. The idea of discrete or quantized nature of energy had deep consequences and resulted in development of quantum mechanics. The quantum theory of optical fields is called *quantum optics*. The construction of lasers in the 1960s gave impulse to rapid development of nonlinear optics with a broad variety of nonlinear optical phenomena that have been

Modern Nonlinear Optics, Part 1, Second Edition, Advances in Chemical Physics, Volume 119, Edited by Myron W. Evans. Series Editors I. Prigogine and Stuart A. Rice.
ISBN 0-471-38930-7

experimentally observed and described theoretically and now are the subject of textbooks [1,2]. In early theoretical descriptions of nonlinear optical phenomena, the quantum nature of optical fields has been ignored on the grounds that laser fields are so strong, that is, the number of photons associated with them are so huge, that the quantum properties assigned to individual photons have no chances to manifest themselves. However, it turned out pretty soon that quantum noise associated with the vacuum fluctuations can have important consequences for the course of nonlinear phenomena. Moreover, it appeared that the quantum noise itself can change essentially when the quantum field is subject to the nonlinear transformation that is the essence of any nonlinear process. The quantum states with reduced quantum noise for a particular physical quantity can be prepared in various nonlinear processes. Such states have no classical counterparts; that is, the results of some physical measurements cannot be explained without explicit recall to the quantum character of the field. The methods of theoretical description of quantum noise are the subject of Gardiner's book [3]. This chapter is not intended as a presentation of general methods that can be found in the book; rather, we want to compare the results obtained with a few chosen methods for the two, probably most important, nonlinear processes: second-harmonic generation and downconversion with quantum pump.

Why have we chosen the second-harmonic generation and the downconversion to illustrate consequences of field quantization, or a role of quantum noise, in nonlinear optical processes? The two processes are at the same time similar and different. Both of them are described by the same interaction Hamiltonian, so in a sense they are similar and one can say that they show different faces of the same process. However, they are also different, and the difference between them consists in the different initial conditions. This difference appears to be very important, at least at early stages of the evolution, and the properties of the fields produced in the two processes are quite different. With these two best-known and practically very important examples of nonlinear optical processes, we would like to discuss several nonclassical effects and present the most common theoretical approaches used to describe quantum effects. The chapter is not intended to be a complete review of the results concerning the two processes that have been collected for years. We rather want to introduce the reader who is not an expert in quantum optics into this fascinating field by presenting not only the results but also how they can be obtained with presently available computer software. The results are largely illustrated graphically for easier comparisons. In Section II we introduce basic definitions and the most important formulas required for later discussion. Section III is devoted to presentation of results for second-harmonic generation, and Section IV results for downconversion. In the Appendixes A and B we have added examples of computer programs that illustrate usage of really existing software and were

actually used in our calculations. We draw special attention to symbolic calculations and numerical methods, which can now be implemented even on small computers.

II. BASIC DEFINITIONS

In classical optics, a one mode electromagnetic field of frequency ω, with the propagation vector $\mathbf{k}$ and linear polarization, can be represented as a plane wave

$$E(\mathbf{r}, t) = 2E_0 \cos(\mathbf{k} \cdot \mathbf{r} - \omega t + \varphi) \tag{1}$$

where E_0 is the amplitude and φ is the phase of the field. Assuming the linear polarization of the field, we have omitted the unit polarization vector to simplify the notation. Classically, both the amplitude E_0 and the phase φ can be well-defined quantities, with zero noise. Of course, the two quantities can be considered as classical random variables with nonzero variances; thus, they can be noisy in a classical sense, but there is no relation between the two variances and, in principle, either of them can be rendered zero giving the noiseless classical field. Apart from a constant factor, the squared real amplitude, E_0^2, is the intensity of the field. In classical electrodynamics there is no real need to use complex numbers to describe the field. However, it is convenient to work with exponentials rather than cosine and sine functions and the field (1) is usually written in the form

$$E(\mathbf{r}, t) = E^{(+)} e^{i(\mathbf{k} \cdot \mathbf{r} - \omega t)} + E^{(-)} e^{-i(\mathbf{k} \cdot \mathbf{r} - \omega t)} \tag{2}$$

with the complex amplitudes $E^{\pm} = E_0 e^{\pm i\varphi}$. The modulus squared of such an amplitude is the intensity of the field, and the argument is the phase. Both intensity and the phase can be measured simultaneously with arbitrary accuracy.

In quantum optics the situation is dramatically different. The electromagnetic field E becomes a quantum quantity; that is, it becomes an operator acting in a Hilbert space of field states, the complex amplitudes $E^{\pm}$ become the annihilation and creation operators of the electromagnetic field mode, and we have

$$\hat{E} = \sqrt{\frac{\hbar\omega}{2\varepsilon_0 V}} [\hat{a} e^{i(\mathbf{k} \cdot \mathbf{r} - \omega t)} + \hat{a}^+ e^{-i(\mathbf{k} \cdot \mathbf{r} - \omega t)}] \tag{3}$$

with the bosonic commutation rules

$$[\hat{a}, \hat{a}^+] = 1 \tag{4}$$

for the annihilation ($\hat{a}$) and creation ($\hat{a}^+$) operators of the field mode, where ε_0 is the electric permittivity of free space and V is the quantization volume. Because

of laws of quantum mechanics, optical fields exhibit an inherent quantum indeterminacy that cannot be removed for principal reasons no matter how smart we are. The quantity

$$\mathscr{E}_0 = \sqrt{\frac{\hbar\omega}{2\varepsilon_0 V}} \tag{5}$$

appearing in (3) is a measure of the quantum optical noise for a single mode of the field. This noise is present even if the field is in the vacuum state, and for this reason it is usually referred to as the *vacuum fluctuations of the field* [4]. Quantum noise associated with the vacuum fluctuations, which appears because of noncommuting character of the annihilation and creation operators expressed by (4), is ubiquitous and cannot be eliminated, but we can to some extent control this noise by 'squeezing' it in one quantum variable at the expense of "expanding" it in another variable. This noise, no matter how small it is in comparison to macroscopic fields, can have very important macroscopic consequences changing the character of the evolution of the macroscopic fields. We are going to address such questions in this chapter.

The electric field operator (3) can be rewritten in the form

$$\hat{E} = \mathscr{E}_0\left[\hat{Q}\cos(\mathbf{k}\cdot\mathbf{r} - \omega t) + \hat{P}\sin(\mathbf{k}\cdot\mathbf{r} - \omega t)\right] \tag{6}$$

where we have introduced two Hermitian quadrature operators, $\hat{Q}$ and $\hat{P}$, defined as

$$\hat{Q} = \hat{a} + \hat{a}^+, \qquad \hat{P} = -i(\hat{a} - \hat{a}^+) \tag{7}$$

which satisfy the commutation relation

$$[\hat{Q}, \hat{P}] = 2i \tag{8}$$

The two quadrature operators thus obey the Heisenberg uncertainty relation

$$\langle(\Delta\hat{Q})^2\rangle\langle(\Delta\hat{P})^2\rangle \geq 1 \tag{9}$$

where we have introduced the quadrature noise operators

$$\Delta\hat{Q} = \hat{Q} - \langle\hat{Q}\rangle, \qquad \Delta\hat{P} = \hat{P} - \langle\hat{P}\rangle \tag{10}$$

For the vacuum state or a coherent state, which are the minimum uncertainty states, the inequality (9) becomes equality and, moreover, the two variances are equal

$$\langle(\Delta\hat{Q})^2\rangle = \langle(\Delta\hat{P})^2 = 1 \tag{11}$$

The Heisenberg uncertainty relation (9) imposes basic restrictions on the accuracy of the simultaneous measurement of the two quadrature components of the optical field. In the vacuum state the noise is isotropic and the two components have the same level of quantum noise. However, quantum states can be produced in which the isotropy of quantum fluctuations is broken—the uncertainty of one quadrature component, say, $\hat{Q}$, can be reduced at the expense of expanding the uncertainty of the conjugate component, $\hat{P}$. Such states are called *squeezed states* [5,6]. They may or may not be the minimum uncertainty states. Thus, for squeezed states

$$\langle(\Delta\hat{Q})^2\rangle < 1 \quad \text{or} \quad \langle(\Delta\hat{P})^2\rangle < 1 \tag{12}$$

Squeezing is a unique quantum property that cannot be explained when the field is treated as a classical quantity—field quantization is crucial for explaining this effect.

Another nonclassical effect is referred to as *sub-Poissonian photon statistics* (see, e.g., Refs. 7 and 8 and papers cited therein). It is well known that in a coherent state defined as an infinite superposition of the number states

$$|\alpha\rangle = \exp\left(-\frac{|\alpha|^2}{2}\right)\sum_{n=0}^{\infty}\frac{\alpha^n}{\sqrt{n!}}|n\rangle \tag{13}$$

the photon number distribution is Poissonian

$$p(n) = |\langle n|\alpha\rangle|^2 = \exp(-|\alpha|^2)\frac{|\alpha|^{2n}}{n!} = \exp(-\langle\hat{n}\rangle)\frac{\langle\hat{n}\rangle^n}{n!} \tag{14}$$

which means

$$\langle(\Delta\hat{n})^2\rangle = \langle\hat{n}^2\rangle - \langle\hat{n}\rangle^2 = \langle\hat{n}\rangle \tag{15}$$

If the variance of the number of photons is smaller than its mean value, the field is said to exhibit the sub-Poissonian photon statistics. This effect is related to the second-order intensity correlation function

$$G^{(2)}(\tau) = \langle{:}\hat{n}(t)\hat{n}(t+\tau){:}\rangle = \langle\hat{a}^+(t)\hat{a}^+(t+\tau)\hat{a}(t+\tau)\hat{a}(t)\rangle \tag{16}$$

where $::$ indicate the normal order of the operators. This function describes the probability of counting a photon at t and another one at $t+\tau$. For stationary fields, this function does not depend on t but solely on τ. The normalized

second-order correlation function, or second-order degree of coherence, is defined as

$$g^{(2)}(\tau) = \frac{G^{(2)}(\tau)}{\langle \hat{n} \rangle^2} \tag{17}$$

If $g^{(2)}(\tau) < g^{(2)}(0)$, the probability of detecting the second photon decreases with the time delay τ, indicating *bunching* of photons. On the other hand, if $g^{(2)}(\tau) > g^{(2)}(0)$, we have the effect of *antibunching* of photons. Photon antibunching is another signature of quantum character of the field. For $\tau = 0$, we have

$$g^{(2)}(0) = \frac{\langle \hat{a}^+ \hat{a}^+ \hat{a}\, \hat{a} \rangle}{\langle \hat{a}^+ \hat{a} \rangle^2} = \frac{\langle \hat{n}(\hat{n} - 1) \rangle}{\langle \hat{n} \rangle^2} = 1 + \frac{\langle (\Delta \hat{n})^2 \rangle - \langle \hat{n} \rangle}{\langle \hat{n} \rangle^2} \tag{18}$$

which gives the relation between the photon statistics and the second-order correlation function. Another convenient parameter describing the deviation of the photon statistics from the Poissonian photon number distribution is the Mandel q parameter defined as [9]

$$q = \frac{\langle (\Delta \hat{n})^2 \rangle}{\langle \hat{n} \rangle} - 1 = \langle \hat{n} \rangle (g^{(2)}(0) - 1) \tag{19}$$

Negative values of this parameter indicate sub-Poissonian photon statistics, namely, nonclassical character of the field. One obvious example of the nonclassical field is a field in a number state $|n\rangle$ for which the photon number variance is zero, and we have $g^{(2)}(0) = 1 - 1/n$ and $q = -1$. For coherent states, $g^{(2)}(0) = 1$ and $q = 0$. In this context, coherent states draw a somewhat arbitrary line between the quantum states that have "classical analogs" and the states that do not have them. The coherent states belong to the former category, while the states for which $g^{(2)}(0) < 1$ or $q < 0$ belong to the latter category. This distinction is better understood when the Glauber–Sudarshan quasidistribution function $P(\alpha)$ is used to describe the field.

The coherent states (13) can be used as a basis to describe states of the field. In such a basis for a state of the field described by the density matrix ρ, we can introduce the quasidistribution function $P(\alpha)$ in the following way:

$$\rho = \int d^2\alpha\, P(\alpha) |\alpha\rangle\langle\alpha| \tag{20}$$

where $d^2\alpha = d\,\mathrm{Re}(\alpha)\, d\,\mathrm{Im}(\alpha)$. In terms of $P(\alpha)$, the expectation value of the normally ordered products (creation operators to the left and annihilation

operators to the right) has the form

$$\langle(\hat{a}^+)^m\hat{a}^n\rangle = \mathrm{Tr}\,[\rho(\hat{a}^+)^m\hat{a}^n] = \int d^2\alpha\, P(\alpha)(\alpha^*)^m\alpha^n \tag{21}$$

For a coherent state $|\alpha_0\rangle$, $\rho = |\alpha_0\rangle\langle\alpha_0|$, and the quasiprobability distribution $P(\alpha) = \delta^{(2)}(\alpha - \alpha_0)$ giving $\langle(a^+)^m a^n\rangle = (\alpha^*)^m\alpha^n\rangle$. When $P(\alpha)$ is a well-behaved, positive definite function, it can be considered as a probability distribution function of a classical stochastic process, and the field with such a P function is said to have "classical analog." However, the P function can be highly singular or can take negative values, in which case it does not satisfy requirements for the probability distribution, and the field states with such a P function are referred to as *nonclassical states*.

From the definition (13) of coherent state it is easy to derive the completeness relation

$$\frac{1}{\pi}\int d^2\alpha\,|\alpha\rangle\langle\alpha| = 1 \tag{22}$$

and find that the coherent states do not form an orthonormal set

$$|\langle\alpha|\beta\rangle|^2 = \exp(-|\alpha - \beta|^2) \tag{23}$$

and only for $|\alpha - \beta|^2 \gg 1$ they are approximately orthogonal. In fact, coherent states form an overcomplete set of states.

To see the nonclassical character of squeezed states better, let us express the variance $\langle(\Delta\hat{Q})^2\rangle$ in terms of the P function

$$\begin{aligned}\langle(\Delta\hat{Q})^2\rangle &= \langle(\hat{a} + \hat{a}^+)^2\rangle - \langle(\hat{a} + \hat{a}^+)\rangle^2 \\ &= \langle\hat{a}^2 + \hat{a}^{+2} + 2\hat{a}^+\hat{a} + 1\rangle - \langle\hat{a} + \hat{a}^+\rangle^2 \\ &= 1 + \int d^2\alpha\, P(\alpha)[(\alpha + \alpha^*)^2 - \langle\alpha + \alpha^*\rangle^2]\end{aligned} \tag{24}$$

which shows that $\langle(\Delta\hat{Q})^2\rangle < 1$ is possible only if $P(\alpha)$ is not a positive definite function. The unity on the right-hand side of (24) comes from applying the commutation relation (4) to put the formula into its normal form, and it is thus a manifestation of the quantum character of the field ("shot noise").

Similarly, for the photon number variance, we get

$$\begin{aligned}\langle(\Delta\hat{n})^2\rangle &= \langle\hat{n}\rangle + \langle\hat{a}^{+2}\hat{a}^2\rangle - \langle\hat{a}^+\hat{a}\rangle^2 \\ &= \langle\hat{n}\rangle + \int d^2\alpha\, P(\alpha)[|\alpha|^2 - \langle|\alpha|^2\rangle]^2\end{aligned} \tag{25}$$

Again, $\langle(\Delta\hat{n})^2\rangle < \langle\hat{n}\rangle$ only if $P(\alpha)$ is not positive definite, and thus sub-Poissonian photon statistics is a nonclassical feature.

In view of (24), one can write

$$\langle(\Delta\hat{Q})^2\rangle = 1 + \langle: (\Delta\hat{Q})^2 :\rangle, \qquad \langle(\Delta\hat{P})^2\rangle = 1 + \langle: (\Delta\hat{P})^2 :\rangle \tag{26}$$

where : : indicate the normal form of the operator. Using the normal form of the quadrature component variances squeezing can be conveniently defined by the condition

$$\langle: (\Delta\hat{Q})^2 :\rangle < 0 \quad \text{or} \quad \langle: (\Delta\hat{P})^2 :\rangle < 0 \tag{27}$$

Therefore, whenever the normal form of the quadrature variance is negative, this component of the field is squeezed or, in other words, the quantum noise in this component is reduced below the vacuum level. For classical fields, there is no unity coming from the boson commutation relation, and the normal form of the quadrature component represents true variance of the classical stochastic variable, which must be positive.

The Glauber–Sudarshan P representation of the field state is associated with the normal order of the field operators and is not the only c-number representation of the quantum state. Another quasidistribution that is associated with antinormal order of the operators is the Q representation, or the Husimi function, defined as

$$Q(\alpha) = \frac{1}{\pi}\langle\alpha|\rho|\alpha\rangle \tag{28}$$

and in terms of this function the expectation value of the antinormally ordered product of the field operators is calculated according to the formula

$$\langle\hat{a}^m(\hat{a}^+)^n\rangle = \frac{1}{\pi}\int d^2\alpha\,\langle\alpha|\rho|\alpha\rangle\alpha^m(\alpha^*)^n \tag{29}$$

It is clear from (28) that $Q(\alpha)$ is always positive, since ρ is a positive definite operator. For a coherent state $|\alpha_0\rangle$, $Q(\alpha) = (1/\pi)\exp(-|\alpha - \alpha_0|^2)$ is a Gaussian in the phase space $\{\mathrm{Re}\,\alpha, \mathrm{Im}\,\alpha\}$ which is centered at α_0. The section of this function, which is a circle, represents isotropic noise in the coherent state (the same as for the vacuum). The anisotropy introduced by squeezed states means a deformation of the circle into an ellipse or another shape.

Generally, according to Cahill and Glauber [10], one can introduce the s-parametrized quasidistribution function $\mathscr{W}^{(s)}(\alpha)$ defined as

$$\mathscr{W}^{(s)}(\alpha) = \frac{1}{\pi}\mathrm{Tr}\{\rho\,\hat{T}^{(s)}(\alpha)\} \tag{30}$$

where the operator $\hat{T}^{(s)}(\alpha)$ is given by

$$\hat{T}^{(s)}(\alpha) = \frac{1}{\pi}\int d^2\xi \exp(\alpha\xi^* - \alpha^*\xi)\hat{D}^{(s)}(\xi) \tag{31}$$

and

$$\hat{D}^{(s)}(\xi) = \exp\left(\frac{s\xi^2}{2}\right)\hat{D}(\xi) \tag{32}$$

where $\hat{D}(\xi)$ is the displacement operator and ρ is the density matrix of the field. The operator $\hat{T}^{(s)}(\alpha)$ can be rewritten in the form

$$\hat{T}^{(s)}(\alpha) = \frac{2}{1-s}\sum_{n=0}^{\infty}\hat{D}(\alpha)|n\rangle\left(\frac{s+1}{s-1}\right)^n\langle n|\hat{D}^{+}(\alpha) \tag{33}$$

which gives explicitly its s dependence. So, the s-parametrized quasidistribution function $\mathscr{W}^{(s)}(\alpha)$ has the following form in the number-state basis

$$\mathscr{W}^{(s)}(\alpha) = \frac{1}{\pi}\sum_{m,n}\rho_{mn}\langle n|\hat{T}^{(s)}(\alpha)|m\rangle \tag{34}$$

where the matrix elements of the operator (31) are given by

$$\begin{aligned}\langle n|\hat{T}^{(s)}(\alpha)|m\rangle = {} & \sqrt{\frac{n!}{m!}}\left(\frac{2}{1-s}\right)^{m-n+1}\left(\frac{s+1}{s-1}\right)^n e^{-i(m-n)\theta}|\alpha|^{m-n} \\ & \times \exp\left(-\frac{2|\alpha|^2}{1-s}\right)L_n^{m-n}\left(\frac{4|\alpha|^2}{1-s^2}\right)\end{aligned} \tag{35}$$

in terms of the associate Laguerre polynomials $L_n^{m-n}(x)$. In this equation we have also separated explicitly the phase of the complex number α by writing

$$\alpha = |\alpha|e^{i\theta} \tag{36}$$

The phase θ is the quantity representing the field phase.

With the quasiprobability distributions $\mathscr{W}^{(s)}(\alpha)$, the expectation values of the s-ordered products of the creation and annihilation operators can be obtained by proper integrations in the complex α plane. In particular, for $s = 1, 0, -1$, the s-ordered products are normal, symmetric, and antinormal ordered products of the creation and annihilation operators, and the corresponding distributions are the Glauber–Sudarshan P function, Wigner function, and Husimi Q function. By

virtue of the relation inverse to (34), the field density matrix can be retrieved from the quasiprobability function

$$\rho = \int d^2\alpha\, \hat{T}^{(-s)}(\alpha) W^{(s)}(\alpha) \tag{37}$$

Polar decomposition of the field amplitude, as in (36), which is trivial for classical fields becomes far from being trivial for quantum fields because of the problems with proper definition of the Hermitian phase operator. It was quite natural to associate the photon number operator with the intensity of the field and somehow construct the phase operator conjugate to the number operator. The latter task, however, turned out not to be easy. Pegg and Barnett [11–13] introduced the Hermitian phase formalism, which is based on the observation that in a finite-dimensional state space, the states with well-defined phase exist [14]. Thus, they restrict the state space to a finite $(\sigma + 1)$-dimensional Hilbert space $\mathrm{H}^{(\sigma)}$ spanned by the number states $|0\rangle, |1\rangle, \ldots, |\sigma\rangle$. In this space they define a complete orthonormal set of phase states by

$$|\theta_m\rangle = \frac{1}{\sqrt{\sigma+1}} \sum_{n}^{\sigma} \exp(in\theta_m)|n\rangle\,, \qquad m = 0, 1, \ldots, \sigma \tag{38}$$

where the values of θ_m are given by

$$\theta_m = \theta_0 + \frac{2\pi m}{\sigma + 1} \tag{39}$$

The value of θ_0 is arbitrary and defines a particular basis set of $(\sigma + 1)$ mutually orthogonal phase states. The number state $|n\rangle$ can be expanded in terms of the $|\theta_m\rangle$ phase-state basis as

$$|n\rangle = \sum_{m=0}^{\sigma} |\theta_m\rangle\langle\theta_m|n\rangle = \frac{1}{\sqrt{\sigma+1}} \sum_{m=0}^{\sigma} \exp(-in\theta_m)|\theta_m\rangle \tag{40}$$

From Eqs. (38) and (40) we see that a system in a number state is equally likely to be found in any state $|\theta_m\rangle$, and a system in a phase state is equally likely to be found in any number state $|n\rangle$.

The Pegg–Barnett Hermitian phase operator is defined as

$$\hat{\Phi}_\theta = \sum_{m=0}^{\sigma} \theta_m |\theta_m\rangle\langle\theta_m| \tag{41}$$

Of course, the phase states (38) are eigenstates of the phase operator (40) with the eigenvalues θ_m restricted to lie within a phase window between θ_0 and $\theta_0 + 2\pi\sigma/(\sigma + 1)$. The Pegg–Barnett prescription is to evaluate any observable of interest in the finite basis (38), and only after that to take the limit $\sigma \to \infty$.

Since the phase states (38) are orthonormal, $\langle\theta_m|\theta_{m'}\rangle = \delta_{mm'}$, the kth power of the Pegg–Barnett phase operator (41) can be written as

$$\hat{\Phi}_\theta^k = \sum_{m=0}^{\sigma} \theta_m^k |\theta_m\rangle\langle\theta_m| \tag{42}$$

Substituting Eqs. (38) and (39) into Eq. (41) and performing summation over m yields explicitly the phase operator in the Fock basis:

$$\hat{\Phi}_\theta = \theta_0 + \frac{\sigma\pi}{\sigma + 1} + \frac{2\pi}{\sigma + 1} \sum_{n \neq n'} \frac{\exp[i(n - n')\theta_0]|n\rangle\langle n'|}{\exp[i(n - n')2\pi/(\sigma + 1)] - 1} \tag{43}$$

It is readily apparent that the Hermitian phase operator $\hat{\Phi}_\theta$ has well-defined matrix elements in the number-state basis and does not suffer from the problems as those the original Dirac phase operator suffered. Indeed, using the Pegg–Barnett phase operator (43) one can readily calculate the phase-number commutator [13]

$$[\hat{\Phi}_\theta, \hat{n}] = -\frac{2\pi}{\sigma + 1} \sum_{n \neq n'} \frac{(n - n')\exp[i(n - n')\theta_0]}{\exp[i(n - n')2\pi/(\sigma + 1)] - 1} |n\rangle\langle n'| \tag{44}$$

This equation looks very different from the famous Dirac postulate for the phase-number commutator.

The Pegg–Barnett Hermitian phase formalism allows for direct calculations of quantum phase properties of optical fields. As the Hermitian phase operator is defined, one can calculate the expectation value and variance of this operator for a given state $|f\rangle$. Moreover, the Pegg–Barnett phase formalism allows for the introduction of the continuous phase probability distribution, which is a representation of the quantum state of the field and describes the phase properties of the field in a very spectacular fashion. For so-called physical states, that is, states of finite energy, the Pegg–Barnett formalism simplifies considerably. In the limit as $\sigma \to \infty$ one can introduce the continuous phase distribution

$$P(\theta) = \lim_{\sigma \to \infty} \frac{\sigma + 1}{2\pi} |\langle\theta_m|f\rangle|^2 \tag{45}$$

where $(\sigma + 1)/2\pi$ is the density of states and the discrete variable θ_m is replaced by a continuous phase variable θ. In the number-state basis the

Pegg–Barnett phase distribution takes the form [15]

$$P(\theta) = \frac{1}{2\pi}\left\{1 + 2\mathrm{Re}\sum_{m>n}\rho_{mn}\exp[-i(m-n)\theta]\right\} \tag{46}$$

where $\rho_{mn} = \langle m|\rho|n\rangle$ are the density matrix elements in the number-state basis. The phase distribution (46) is 2π-periodic, and for all states with the density matrix diagonal in the number-state basis, the phase distribution is uniform over the 2π-wide phase window. Knowing the phase distribution makes the calculation of the phase operator expectation values quite simple; it is simply the calculation of all integrals over the continuous phase variable θ. For example,

$$\langle f|\hat{\Phi}_\theta^k|f\rangle = \int_{\theta_0}^{\theta_0+2\pi} d\theta\,\theta^k P(\theta) \tag{47}$$

When the phase window is chosen in such a way that the phase distribution is symmetrized with respect to the initial phase of the partial phase state, the phase variance is given by the formula

$$\langle(\Delta\hat{\Phi}_\theta)^2\rangle = \int_{-\pi}^{\pi} d\theta\,\theta^2 P(\theta) \tag{48}$$

For a partial phase state with the decomposition

$$|f\rangle = \sum_n b_n e^{in\varphi}|n\rangle \tag{49}$$

the phase variance has the form

$$\langle(\Delta\hat{\Phi}_\theta)^2\rangle = \frac{\pi^2}{3} + 4\sum_{n>k} b_n b_k \frac{(-1)^{n-k}}{(n-k)^2} \tag{50}$$

The value $\pi^2/3$ is the variance for the uniformly distributed phase, as in the case of a single-number state.

On integrating the quasiprobability distribution $\mathscr{W}^{(s)}(\alpha)$, given by (34), over the "radial" variable $|\alpha|$, we get a "phase distribution" associated with this quasiprobability distribution. The s-parametrized phase distribution is thus given by

$$P^{(s)}(\theta) = \int_0^\infty d|\alpha|\,\mathscr{W}^{(s)}(\alpha)|\alpha| \tag{51}$$

which, after performing of the integrations, gives the formula similar to the Pegg–Barnett phase distribution

$$P^{(s)}(\theta) = \frac{1}{2\pi}\left\{1 + 2\mathrm{Re}\sum_{m>n} \rho_{mn} e^{-i(m-n)\theta} G^{(s)}(m,n)\right\} \tag{52}$$

The difference between the Pegg–Barnett phase distribution (46) and the distribution (52) lies in the coefficients $G^{(s)}(m,n)$, which are given by [16]

$$G^{(s)}(m,n) = \left(\frac{2}{1-s}\right)^{(m+n)/2} \sum_{l=0}^{\min(m,n)} (-1)^l \left(\frac{1+s}{2}\right)^l \times \sqrt{\binom{n}{l}\binom{m}{l}} \frac{\Gamma\left(\dfrac{m+n}{2} - l + 1\right)}{\sqrt{(m-l)!(n-l)!}} \tag{53}$$

The phase distributions obtained by integration of the quasidistribution functions are different for different s, and all of them are different from the Pegg–Barnett phase distribution. The Pegg–Barnett phase distribution is always positive while the distribution associated with the Wigner distribution ($s = 0$) may take negative values. The distribution associated with the Husimi Q function is much broader than the Pegg–Barnett distribution, indicating that some phase information on the particular quantum state has been lost. Quantum phase fluctuations as fluctuations associated with the operator conjugate to the photon-number operator are important for complete picture of the quantum noise of the optical fields (for more details, see, e.g., Refs. 16 and 17).

III. SECOND-HARMONIC GENERATION

Second-harmonic generation, which was observed in the early days of lasers [18] is probably the best known nonlinear optical process. Because of its simplicity and variety of practical applications, it is a starting point for presentation of nonlinear optical processes in the textbooks on nonlinear optics [1,2]. Classically, the second-harmonic generation means the appearance of the field at frequency 2ω (second harmonic) when the optical field of frequency ω (fundamental mode) propagates through a nonlinear crystal. In the quantum picture of the process, we deal with a nonlinear process in which two photons of the fundamental mode are annihilated and one photon of the second harmonic is created. The classical treatment of the problem allows for closed-form solutions with the possibility of energy being transferred completely into the second-harmonic mode. For quantum fields, the closed-form analytical solution of the

problem has not been found unless some approximations are made. The early numerical solutions [19,20] showed that quantum fluctuations of the field prevent the complete transfer of energy into the second harmonic and the solutions become oscillatory. Later studies showed that the quantum states of the field generated in the process have a number of unique quantum features such as photon antibunching [21] and squeezing [9,22] for both fundamental and second harmonic modes (for a review and literature, see Ref. 23). Nikitin and Masalov [24] discussed the properties of the quantum state of the fundamental mode by calculating numerically the quasiprobability distribution function $Q(\alpha)$. They suggested that the quantum state of the fundamental mode evolves, in the course of the second-harmonic generation, into a superposition of two macroscopically distinguishable states, similar to the superpositions obtained for the anharmonic oscillator model [25–28] or a Kerr medium [29,30]. Bajer and Lisoněk [31] and Bajer and Peřina [32] have applied a symbolic computation approach to calculate Taylor series expansion terms to find evolution of nonlinear quantum systems. A quasiclassical analysis of the second harmonic generation has been done by Alvarez-Estrada et al. [33]. Phase properties of fields in harmonics generation have been studied by Gantsog et al. [34] and Drobný and Jex [35]. Bajer et al. [36] and Bajer et al. [37] have discussed the sub-Poissonian behavior in the second- and third-harmonic generation. More recently, Olsen et al. [38,38] have investigated quantum-noise-induced macroscopic revivals in second-harmonic generation and criteria for the quantum nondemolition measurement in this process.

Quantum description of the second harmonic generation, in the absence of dissipation, can start with the following model Hamiltonian

$$\hat{H} = \hat{H}_0 + \hat{H}_I \tag{54}$$

where

$$\hat{H}_0 = \hbar\omega\hat{a}^+\hat{a} + 2\hbar\omega\hat{b}^+\hat{b}\,, \qquad \hat{H}_I = \hbar\kappa(\hat{a}^2\hat{b}^+ + \hat{a}^{+2}\hat{b}) \tag{55}$$

and $\hat{a}$ ($\hat{a}^+$), $\hat{b}$ ($\hat{b}^+$) are the annihilation (creation) operators of the fundamental mode of frequency ω and the second harmonic mode at frequency 2ω, respectively. The coupling constant κ, which is real, describes the coupling between the two modes. Since $\hat{H}_0$ and $\hat{H}_I$ commute, there are two constants of motion: $\hat{H}_0$ and $\hat{H}_I$, $\hat{H}_0$ determines the total energy stored in both modes, which is conserved by the interaction $\hat{H}_I$. The free evolution associated with the Hamiltonian $\hat{H}_0$ leads to $\hat{a}(t) = \hat{a}(0)\exp(-i\omega t)$ and $\hat{b}(t) = \hat{b}(0)\exp(-i2\omega t)$. This trivial exponential evolution can always be factored out and the important part of the evolution described by the interaction Hamiltonian $\hat{H}_I$, for the slowly

varying operators in the Heisenberg picture, is given by a set of equations

$$\frac{d}{dt}\hat{a}(t) = \frac{1}{i\hbar}[\hat{a}, \hat{H}_I] = -2i\kappa\,\hat{a}^+(t)\hat{b}(t)$$
$$\frac{d}{dt}\hat{b}(t) = \frac{1}{i\hbar}[\hat{b}, \hat{H}_I] = -i\kappa\,\hat{a}^2(t) \tag{56}$$

where for notational convenience we use the same notation for the slowly varying operators as for the original operators — it is always clear from the context which operators are considered. In deriving the equations of motion (56), it is assumed that the operators associated with different modes commute, while for the same mode they obey the bosonic commutation rules (4).

Usually, the second-harmonic generation is considered as a propagation problem, not a cavity field problem, and the evolution variable is rather the path z the two beams traveled in the nonlinear medium. In the simplest, discrete two mode description of the process the transition from the cavity to the propagation problem is done by the replacement $t = -z/v$, where v denotes the velocity of the beams in the medium (we assume perfect matching conditions). We will use here time as the evolution variable, but it is understood that it can be equally well the propagation time in the propagation problem. So, we basically consider an idealized, one-pass problem. In fact, in the cavity situation the classical field pumping the cavity as well as the cavity damping must be added into the simple model to make it more realistic. Quantum theory of such a model has been developed by Drummond et al. [39,40]. Another interesting possibility is to study the second harmonic generation from the point of view of the chaotic behavior [41]. Such effects,however, will not be the subject of our concern here.

A. Classical Fields

Before we start with quantum description, let us recollect the classical solutions which will be used later in the method of classical trajectories to study some quantum properties of the fields. Equations (56) are valid also for classical fields after replacing the field operators $\hat{a}$ and $\hat{b}$ by the c-number field amplitudes α and β, which are generally complex numbers. They can be derived from the Maxwell equations in the slowly varying amplitude approximation [1] and have the form.

$$\frac{d}{dt}\alpha(t) = -2i\kappa\alpha^*(t)\beta(t)$$
$$\frac{d}{dt}\beta(t) = -i\kappa\alpha^2(t) \tag{57}$$

For classical fields the closed-form analytical solutions to equations (57) are known. Assuming that initially there is no second-harmonic field ($\beta(0) = 0$),

and the fundamental field amplitude is real and equal to $\alpha(0) = \alpha_0$ the solutions for the classical amplitudes of the second harmonic and fundamental modes are given by [1]

$$\alpha(t) = \alpha_0 \operatorname{sech}(\sqrt{2}\,\alpha_0 \kappa t)$$
$$\beta(t) = \frac{\alpha_0}{\sqrt{2}} \tanh(\sqrt{2}\,\alpha_0 \kappa t) \tag{58}$$

The solutions (58) are monotonic and eventually all the energy present initially in the fundamental mode is transferred to the second-harmonic mode.

In a general case, when both modes initially have nonzero amplitudes, $\alpha_0 \neq 0$ and $\beta_0 \neq 0$, introducing $\alpha = |\alpha| e^{i\phi_a}$ and $\beta = |\beta| e^{i\phi_b}$, we obtain the following set of equations:

$$\frac{d}{dt}|\alpha| = -2\kappa |\alpha||\beta| \sin\vartheta$$
$$\frac{d}{dt}|\beta| = \kappa |\alpha|^2 \sin\vartheta$$
$$\frac{d}{dt}\vartheta = \kappa \left(\frac{|\alpha|^2}{|\beta|} - 4|\beta| \right) \cos\vartheta$$
$$\frac{d}{dt}\phi_a = -2\kappa |\beta| \cos\vartheta$$
$$\frac{d}{dt}\phi_b = -\kappa \frac{|\alpha|^2}{|\beta|} \cos\vartheta \tag{59}$$

where $\vartheta = 2\phi_a - \phi_b$. The system (59) has two integrals of motion

$$C_0 = |\alpha|^2 + 2|\beta|^2, \qquad C_I = |\alpha|^2 |\beta| \cos\vartheta \tag{60}$$

which are classical equivalents of the quantum constants of motion $\hat{H}_0$ and $\hat{H}_I$ ($C_0 = \langle \hat{H}_0 \rangle$, $C_I = \langle \hat{H}_I \rangle$). Depending on the values of the constants of motion C_0 and C_I, the dynamics of the system (59) can be classified into several categories [42,43]:

1. *Phase-stable* motion, $C_I = 0$, in which the phases of each mode are preserved and the modes move radially in the phase space. The phase difference ϑ is also preserved, which appears for $\cos\vartheta = 0$ and $\vartheta = \pm\pi/2$. The solutions (58) belong to this category.
2. *Phase-changing* motion, $C_I \neq 0$, in which the dynamics of each mode involves both radial and phase motion. In this case both modes must be initially excited and their phase difference cannot be equal to $\pm\pi/2$.

3. *Phase-difference-stable* motion, which is a special case of the phase-changing motion that preserves the phase difference ϑ between the modes even though the phases of individual modes change. This corresponds to the *no-energy-exchange* regime when $\sin\vartheta = 0$ and the initial amplitudes of the modes are preserved.

Introducing new (scaled) variables

$$u_a = |\alpha|/\sqrt{C_0}, \qquad u_b = \sqrt{2}|\beta|/\sqrt{C_0}, \qquad u_a^2 + u_b^2 = 1 \tag{61}$$

$$\tau = \sqrt{2C_0}\,\kappa t \tag{62}$$

the set of equations (59) can be rewritten in the form

$$\begin{aligned}
\frac{d}{d\tau}u_a &= -u_a u_b \sin\vartheta \\
\frac{d}{d\tau}u_b &= u_a^2 \sin\vartheta \\
\frac{d}{d\tau}\vartheta &= \left(\frac{u_a^2}{u_b} - 2u_b\right)\cos\vartheta \\
\frac{d}{d\tau}\phi_a &= -u_b \cos\vartheta \\
\frac{d}{d\tau}\phi_b &= -\frac{u_a^2}{u_b}\cos\vartheta
\end{aligned} \tag{63}$$

Solutions to the set of equations (63) describe the evolution of the fields with the fundamental as well as second-harmonic frequencies.

From (60) we have

$$\cos\vartheta = \frac{\epsilon}{u_a^2 u_b} \tag{64}$$

where the constant of motion ϵ is defined by

$$\epsilon = \frac{\sqrt{2}C_I}{C_0^{3/2}} = u_a^2(0)u_b(0)\cos\vartheta(0) \tag{65}$$

From (63) and (64) one easily obtains the closed-form equations for the intensities $n_a = u_a^2$ and $n_b = u_b^2$ of the two modes

$$-\frac{dn_a}{d\tau} = \frac{dn_b}{d\tau} = 2\sqrt{n_b(1-n_b)^2 - \epsilon^2} \tag{66}$$

where $n_b = 1 - n_a$. Since the normalized variable n_a must be less, than or equal to unity, the maximum value that can be obtained by ϵ^2 is equal to $\frac{4}{27}$ (for $\cos\vartheta = 1$). From (66) we immediately obtain

$$2\,d\tau = \frac{dn_b}{\sqrt{n_b(1-n_b)^2 - \epsilon^2}} \tag{67}$$

which can be integrated, giving

$$2\tau = \int \frac{dn_b}{\sqrt{n_b(1-n_b)^2 - \epsilon^2}} \tag{68}$$

For $\epsilon = 0$, the integral on the right-hand side (r.h.s.) of (68) is elementary and has the form

$$\int \frac{dn_b}{\sqrt{n_b(1-n_b)^2}} = \ln\frac{1+\sqrt{n_b}}{1-\sqrt{n_b}} \tag{69}$$

In this case we get the well-known classical solution for the intensity of the second harmonic[1]

$$n_b(\tau) = \tanh^2\tau \tag{70}$$

which is a monotonic function of the scaled time $\tau = \sqrt{2C_0}\kappa t$. For $\epsilon \neq 0$ ($C_I \neq 0$), the r.h.s. of (68) is not elementary and the character of solution depends on the roots of the third order polynomial under the square root. Depending on the value of

$$\Delta = \epsilon^2\left(\epsilon^2 - \frac{4}{27}\right) \tag{71}$$

the polynomial has three different real roots ($\Delta < 0$) and two real roots, one of which is double ($\Delta = 0$). The third case with $\Delta > 0$, in which the polynomial has one real root and two complex conjugate roots, is excluded on physical grounds since $\epsilon^2 \leq \frac{4}{27}$.

In case of three different real roots $n_{b1} < n_{b2} < n_{b3}$ ($\Delta < 0$ or $\epsilon^2 < \frac{4}{27}$), we can effect a substitution

$$n_b = n_{b1} + (n_{b2} - n_{b1})\sin^2\phi \tag{72}$$

which leads to the elliptical integral

$$\int \frac{dn_b}{\sqrt{n_b(1-n_b)^2-\epsilon^2}} = \frac{2}{\sqrt{n_{b3}-n_{b1}}} \int \frac{d\phi}{\sqrt{1-k^2\sin^2\phi}} \tag{73}$$

where

$$k^2 = \frac{n_{b2}-n_{b1}}{n_{b3}-n_{b1}} \tag{74}$$

and we get from (68) and (73)

$$\sqrt{n_{b3}-n_{b1}}\,\tau = \int \frac{d\phi}{\sqrt{1-k^2\sin^2\phi}} \tag{75}$$

Using the definitions of the Jacobi elliptic functions we have

$$\sin\phi = \mathrm{sn}\left(\sqrt{n_{b3}-n_{b1}}\,\tau \mid k^2\right) \tag{76}$$

and inserting (76) into (72) we obtain the solution

$$n_b(\tau) = n_{b1} + (n_{b2}-n_{b1})\,\mathrm{sn}^2\left(\sqrt{n_{b3}-n_{b1}}\,\tau \mid k^2\right) \tag{77}$$

where sn is the Jacobi elliptic function sinusamplitude. The solution (77) is a periodic function of the scaled time τ with the period depending on the value of k^2. This means that even very small ϵ makes the solution periodic. The values of $n_b(\tau)$ are restricted to the region between the two smallest roots of the third order polynomial $n_{b1} \le n_b(\tau) \le n_{b2}$. To illustrate the behavior of the classical solutions, we plot in Fig. 1 the time evolution of the intensities of the two modes, $n_a(\tau)$ and $n_b(\tau)$, for the case when the second-harmonic mode is initially weak with respect to the fundamental mode ($n_b(0) = 0.001$) and the initial phases are both zeros ($\phi_a(0) = \phi_b(0) = 0$). In this case the constant of motion $\epsilon = 0.0316$. We see the regular periodic oscillations of the two intensities.

In the limiting case, for which $k = 1$, we have $n_{b1} = 0$, $n_{b2} = n_{b3} = 1$, and $\mathrm{sn}(x \mid 1) = \tanh(x)$ which is the phase-stable motion case and reproduces the classical result (70). The other limiting case appears when $k = 0$, which corresponds to the situation with $\epsilon^2 = \frac{4}{27}$ or $|\alpha|^2 = 4|\beta|^2$ ($n_{b1} = n_{b2} = \frac{1}{3}$, $n_{b3} = \frac{4}{3}$). This is the phase-difference stable motion, or no-energy-exchange, case in which the solution is constant $n_b(\tau) = \frac{1}{3}$. This case has been discussed by Bajer et al. [36]. Thus the two extreme cases, $k = 1$ and $k = 0$, of the general solution (77) correspond to the phase-stable and phase-difference-stable

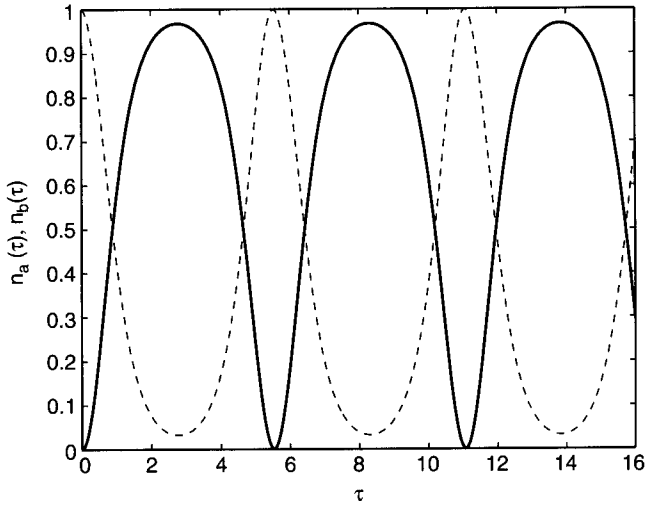

Figure 1. Intensities $n_a(\tau)$ (dashed line) and $n_b(\tau)$ (solid line) of the fundamental and second-harmonic modes for $n_b(0) = 0.001$, $\phi_a(0) = \phi_b(0) = 0$ ($\epsilon = 0.0316$).

motions in the phase space and they are special cases of the general case of the phase changing motion of the system.

The solution (77) for radial variables $u_a(\tau) = \sqrt{n_a(\tau)}$ and $u_b(\tau) = \sqrt{n_b(\tau)}$ must be supplemented with the corresponding solution for the phase variables $\phi_a(\tau)$ and $\phi_b(\tau)$ in order to find the trajectory in the phase space. The equations governing the evolution of the individual phases of the two modes can be rewritten in the form

$$\frac{d}{d\tau}\phi_a = -\frac{\epsilon}{n_a}, \qquad \frac{d}{d\tau}\phi_b = -\frac{\epsilon}{n_b} \tag{78}$$

where ϵ is given by (65). Of course, in the phase-stable regime ($\epsilon = 0$) both phases individually, and obviously the phase difference ϑ, are preserved. In Fig. 2 we have shown the evolution of the phases for the case of weak initial excitation of the second-harmonic mode. The initial values are same as in Fig. 1. Comparing Fig. 1 with Fig. 2, it is seen that there is a jump of the phase $\phi_a(\tau)$ by $\pi/2$ whenever the intensity $n_a(\tau)$ reaches its minimum and a jump by π of the phase $\phi_b(\tau)$ when $n_b(\tau)$ reaches its minimum. The phase difference $\vartheta(\tau) = 2\phi_a(\tau) - \phi_b(\tau)$ jumps between the values $\pm\pi/2$. To plot these figures, we have solved numerically the set of equations (63).

Solutions of equations (66) and (78), or equivalently the set (63), for given initial values describe the deterministic trajectories in the phase space for both

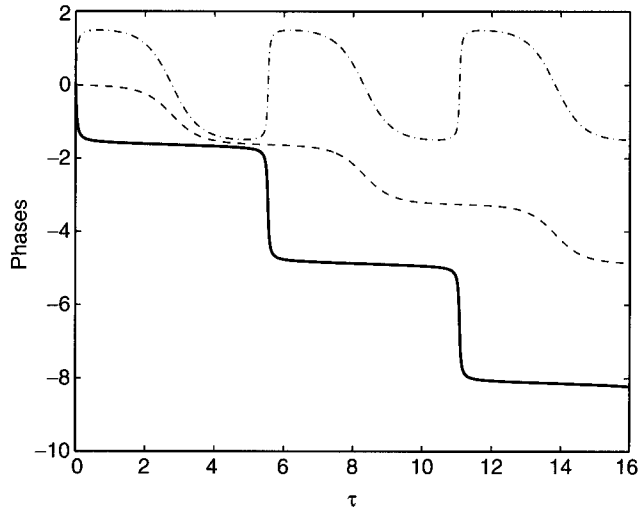

Figure 2. Evolution of the individual phases $\phi_a(\tau)$ (dashed line), $\phi_b(\tau)$ (solid line), and the phase difference $\vartheta(\tau)$ (dashed–dotted line). Initial values are same as in Fig. 1.

modes, the mode at frequency ω and the mode at frequency 2ω, in a general case of the system that describes coupling of the two modes via the $\chi^{(2)}$ nonlinearity. It is a matter of initial conditions whether we have a purely second-harmonic generation case $[n_b(0) = 0,\ n_a(0) = 1]$ or a purely downconversion case $[n_a(0) = 0,\ n_b(0) = 1]$. It is clear from (63) that for the purely downconversion regime $[u_a(0) = 0]$ the classical description does not allow for generating signal at the fundamental frequency from zero initial value. The quantum fluctuations are necessary to obtain such a signal. In a general case both processes take place simultaneously and compete with each other. If the initial amplitudes are well defined, that is, there is no classical noise, the amplitudes at time τ are also well defined. For quantum fields, however, the situation is different because of the inherent quantum noise associated with the vacuum fluctuations. Some quantum features, however, can be simulated with classical trajectories when the initial fields are chosen as random Gaussian variables with appropriately adjusted variances, and examples of such simulations will be shown later.

B. Linearized Quantum Equations

Assuming that the quantum noise is small in comparison to the mean values of the field amplitudes, one can introduce the operators

$$\Delta\hat{a} = \hat{a} - \langle\hat{a}\rangle\,, \qquad \Delta\hat{b} = \hat{b} - \langle\hat{b}\rangle \tag{79}$$

which describe the quantum fluctuations. On inserting the fluctuation operators (79) into the original evolution equations (56) and keeping only the linear terms in the quantum fluctuations, we get the equations

$$\frac{d}{dt}\Delta\hat{a} = -2i\kappa(\Delta\hat{a}^{+}\langle\hat{b}\rangle + \langle\hat{a}^{+}\rangle\Delta\hat{b})$$
$$\frac{d}{dt}\Delta\hat{b} = -2i\kappa\langle\hat{a}\rangle\Delta\hat{a} \tag{80}$$

where $\langle\hat{a}\rangle$ and $\langle\hat{b}\rangle$ are the solutions for the mean fields and can be identified with the classical solutions. With the scaled variables (61) and (62) we can rewrite equations (80) in the form

$$\frac{d}{d\tau}\Delta\hat{a} = -i(\Delta\hat{a}^{+}u_b\,e^{i\phi_b} + \sqrt{2}\,u_a\,e^{-i\phi_a}\Delta\hat{b})$$
$$\frac{d}{d\tau}\Delta\hat{b} = -i\sqrt{2}\,u_a\,e^{i\phi_a}\Delta\hat{a} \tag{81}$$

where $u_a = u_a(\tau)$, $u_b = u_b(\tau)$, $\phi_a = \phi_a(\tau)$, and $\phi_b = \phi_b(\tau)$ are the solutions of classical equations (66) and (78).

The analysis becomes easier if we introduce the following quadrature noise operators [44,45] (for further comparisons, we adjust the phase in quadrature definitions for the second harmonic mode in such a way as to take into account that $\vartheta = 2\phi_a - \phi_b = \pi/2$)

$$\Delta\hat{Q}_a(\tau) = \Delta\hat{a}(\tau)e^{-i\phi_a(\tau)} + \Delta\hat{a}^{+}(\tau)e^{i\phi_a(\tau)}$$
$$\Delta\hat{P}_a(\tau) = -i[\Delta\hat{a}(\tau)e^{-i\phi_a(\tau)} - \Delta\hat{a}^{+}(\tau)e^{i\phi_a(\tau)}]$$
$$\Delta\hat{P}_b(\tau) = \Delta\hat{b}(\tau)e^{-i\phi_b(\tau)} + \Delta\hat{b}^{+}(\tau)e^{i\phi_b(\tau)}$$
$$\Delta\hat{Q}_b(\tau) = i[\Delta\hat{b}(\tau)e^{-i\phi_b(\tau)} - \Delta\hat{b}^{+}(\tau)e^{i\phi_b(\tau)}] \tag{82}$$

for which we get from (81) the following set of equations:

$$\frac{d}{d\tau}\Delta\hat{Q}_a = -\Delta\hat{Q}_a u_b\sin\vartheta - 2\Delta\hat{P}_a u_b\cos\vartheta$$
$$- \Delta\hat{P}_b\sqrt{2}\,u_a\sin\vartheta - \Delta\hat{Q}_b\sqrt{2}u_a\cos\vartheta$$
$$\frac{d}{d\tau}\Delta\hat{P}_a = \Delta\hat{P}_a u_b\sin\vartheta - \Delta\hat{P}_b\sqrt{2}\,u_a\cos\vartheta$$
$$+ \Delta\hat{Q}_b\sqrt{2}\,u_a\sin\vartheta \tag{83}$$

$$\frac{d}{d\tau}\Delta\hat{P}_b = \Delta\hat{Q}_a\sqrt{2}u_a\sin\vartheta + \Delta\hat{P}_a\sqrt{2}\,u_a\cos\vartheta + \Delta\hat{Q}_b\frac{u_a^2}{u_b}\cos\vartheta$$

$$\frac{d}{d\tau}\Delta\hat{Q}_b = \Delta\hat{Q}_a\sqrt{2}u_a\cos\vartheta - \Delta\hat{P}_a\sqrt{2}\,u_a\sin\vartheta - \Delta\hat{P}_b\frac{u_a^2}{u_b}\cos\vartheta$$

In the case of pure second-harmonic generation, that is, for $u_b(0) = 0$ and $u_a(0) = 1$, we have from (59) that $\cos\vartheta = 0$ or $\vartheta = \pm\pi/2$, which implies that, according to (77) for $k = 1$, the scaled intensities obey the equations

$$u_a(\tau) = \operatorname{sech}\tau, \qquad u_b(\tau) = \tanh\tau \tag{84}$$

Inserting $\vartheta = \pi/2$ and the solutions (84) into (83), we arrive at the following system of equations:

$$\begin{aligned}
\frac{d}{d\tau}\Delta\hat{Q}_a &= -\Delta\hat{Q}_a\tanh\tau - \Delta\hat{P}_b\sqrt{2}\operatorname{sech}\tau\\
\frac{d}{d\tau}\Delta\hat{P}_b &= \Delta\hat{Q}_a\sqrt{2}\operatorname{sech}\tau\\
\frac{d}{d\tau}\Delta\hat{P}_a &= \Delta\hat{P}_a\tanh\tau + \Delta\hat{Q}_b\sqrt{2}\operatorname{sech}\tau\\
\frac{d}{d\tau}\Delta\hat{Q}_b &= -\Delta\hat{P}_a\sqrt{2}\operatorname{sech}\tau
\end{aligned} \tag{85}$$

which shows that the quadratures $\Delta\hat{Q}_a$ and $\Delta\hat{P}_b$ of the two modes are coupled together independently from the quadratures $\Delta\hat{P}_a$ and $\Delta\hat{Q}_b$. This splits the system (85) into two independent subsystems. It was shown by Ou [44] that the two systems can be solved analytically, giving

$$\begin{aligned}
\Delta\hat{Q}_a(\tau) &= \Delta\hat{Q}_a(0)(1-\tau\tanh\tau)\operatorname{sech}\tau - \Delta\hat{P}_b(0)\sqrt{2}\tanh\tau\operatorname{sech}\tau\\
\Delta\hat{P}_b(\tau) &= \Delta\hat{Q}_a(0)\frac{1}{\sqrt{2}}(\tanh\tau + \tau\operatorname{sech}^2\tau) + \Delta\hat{P}_b(0)\operatorname{sech}^2\tau\\
\Delta\hat{P}_a(\tau) &= \Delta\hat{P}_a(0)\operatorname{sech}\tau + \Delta\hat{Q}_b(0)\frac{1}{\sqrt{2}}(\sinh\tau + \tau\operatorname{sech}\tau)\\
\Delta\hat{Q}_b(\tau) &= -\Delta\hat{P}_a(0)\sqrt{2}\tanh\tau + \Delta\hat{Q}_b(0)(1-\tau\tanh\tau)
\end{aligned} \tag{86}$$

Now, assuming that the two modes are not correlated at time $\tau = 0$, it is straightforward to calculate the variances of the quadrature field operators and check, according to the definition (12), whether the field is in a squeezed state. If the initial state of the field is a coherent state of the fundamental mode and a vacuum for the second-harmonic mode, $|\psi_0\rangle = |u_a(0)\rangle|0\rangle$, for which we have

$$\langle[\Delta\hat{Q}_a(0)]^2\rangle = \langle[\Delta\hat{Q}_b(0)]^2\rangle = \langle[\Delta\hat{P}_a(0)]^2\rangle = \langle[\Delta\hat{P}_b(0)]^2\rangle = 1 \tag{87}$$

the variances of the two quadrature noise operators are described by the following analytical formulas [44,45]:

$$\begin{aligned}
\langle[\Delta\hat{Q}_a(\tau)]^2\rangle &= (1 - \tau\tanh\tau)^2\,\mathrm{sech}^2\,\tau + 2\tanh^2\tau\,\mathrm{sech}^2\,\tau \\
\langle[\Delta\hat{P}_a(\tau)]^2\rangle &= \mathrm{sech}^2\,\tau + \frac{1}{2}(\sinh\tau + \tau\,\mathrm{sech}\,\tau)^2 \\
\langle[\Delta\hat{Q}_b(\tau)]^2\rangle &= 2\tanh^2\tau + (1 - \tau\tanh\tau)^2 \\
\langle[\Delta\hat{P}_b(\tau)]^2\rangle &= \frac{1}{2}\left(\tanh\tau + \tau\,\mathrm{sech}^2\,\tau\right)^2 + \mathrm{sech}^4\,\tau
\end{aligned} \tag{88}$$

The solutions (88) clearly indicate that the quantum noise present in the initial state of the field, which represents the vacuum fluctuations, undergoes essential changes due to the nonlinear transformation of the field as both modes propagate in the nonlinear medium. As $\tau \to \infty$, we have $\tanh\tau \to 1$, $\mathrm{sech}\,\tau \to 2e^{-\tau}$, and $\sinh\tau \to e^{\tau}/2$, which gives $\langle[\Delta\hat{Q}_a(\tau)]^2\rangle \to 4\tau^2 e^{-2\tau}$, $\langle[\Delta\hat{Q}_b(\tau)]^2\rangle \to \tau^2$, $\langle[\Delta\hat{P}_a(\tau)]^2\rangle \to e^{2\tau}/8$, and $\langle[\Delta\hat{P}_b(\tau)]^2\rangle \to \frac{1}{2}$. According to the definition of squeezing (12), we find that the quadratures $\hat{Q}_a$ and $\hat{P}_b$ become squeezed as τ increases while the other two quadratures, $\hat{P}_a$ and $\hat{Q}_b$, are stretched. For very long times (lengths of the nonlinear medium) the noise in the amplitude quadrature of the fundamental mode is reduced to zero (perfect squeezing), while for the second-harmonic mode it approaches the value $\frac{1}{2}$ (50% squeezing). Quantum fluctuations in the other quadratures of both modes explode to infinity as τ goes to infinity. Of course, we have to keep in mind that the results have been obtained from the linearized equations that require quantum fluctuations to be small. In Fig. 3a we have shown the evolution of the quadrature variances $\langle[\Delta\hat{Q}_a(\tau)]^2\rangle$ and $\langle[\Delta\hat{P}_b(\tau)]^2\rangle$ exhibiting squeezing of quantum fluctuations in both fundamental and second harmonic-modes. With dotted lines the classical amplitudes of the two modes are marked for reference. The value of unity for the quadrature variances sets the level of vacuum fluctuations (coherent states experience the same fluctuations), and we find that indeed the quantum noise can be suppressed below the vacuum level in the amplitude quadrature $\langle[\Delta\hat{Q}_a(\tau)]^2\rangle$ of the fundamental mode and the phase quadrature $\langle[\Delta\hat{P}(\tau)]^2\rangle$ of the harmonic mode. It becomes possible at the expense of increased fluctuations in the other quadratures as to preserve the

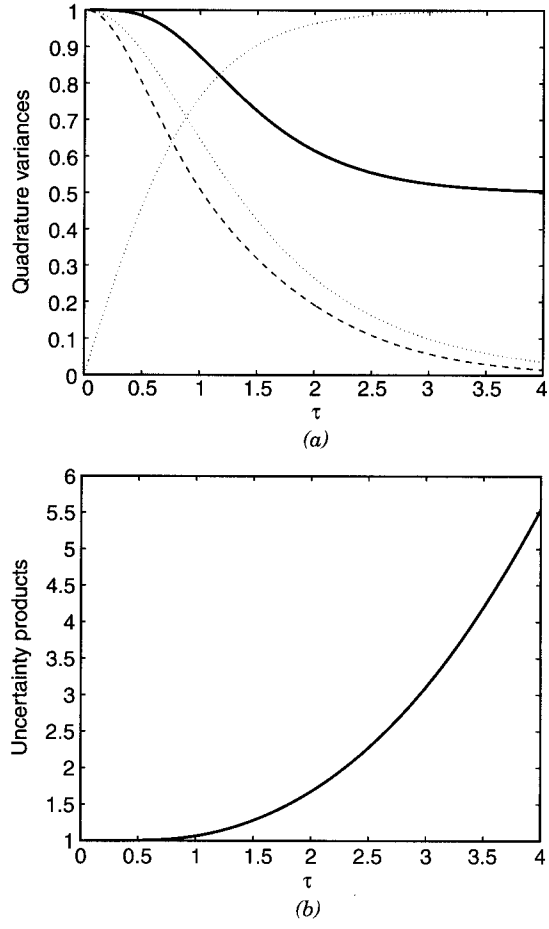

Figure 3. (a) Variances $\langle[\Delta\hat{Q}_a(\tau)]^2\rangle$ (dashed line) and $\langle[\Delta\hat{P}_a(\tau)]^2\rangle$ (solid line) [for reference, the amplitudes $u_a(\tau)$ and $u_b(\tau)$ are marked with dotted lines]; (b) uncertainty products.

validity of the Heisenberg uncertainty relation (9). We have

$$\begin{aligned}\langle[\Delta\hat{Q}_a(\tau)]^2\rangle\langle[\Delta\hat{P}_a(\tau)]^2\rangle &= \langle[\Delta\hat{Q}_b(\tau)]^2\rangle\langle[\Delta\hat{P}_b(\tau)]^2\rangle \\ &= \operatorname{sech}^2(\tau)[2\tanh^2\tau + (1-\tau\tanh\tau)^2] \\ &\quad \times \left[\operatorname{sech}^2\tau + \frac{1}{2}(\sinh\tau + \tau\operatorname{sech}\tau)^2\right] \qquad (89)\end{aligned}$$

and as $\tau \to \infty$ both uncertainty products are divergent as $\tau^2/2$. The evolution of the uncertainty products is illustrated in Fig. 3b. Since, except for the initial value, the value of the uncertainty product is larger than unity, the quantum states produced in the second-harmonic generation process are not the minimum uncertainty states.

The linear approximation to the quantum noise equations presented in this section shows that even in linear approximation the inherent property of quantum fields — the vacuum fluctuations which are ubiquitous and always present — undergo essential changes when transformed nonlinearly. The linearized solutions suggest that perfect squeezing (zero fluctuations) is possible in the fundamental mode for long evolution times (long interaction lengths). This means that one can produce highly nonclassical states of light in such a process. Later we will see to what extent we can trust in the linear approximation.

C. Symbolic Calculations

The linear approximation with respect to quantum noise operators, which assumes that the mean values of the fields evolve according to the classical equations and the quantum noise represents only small fluctuations around the classical solutions is a way to solve the operator equations (56). Another alternative is to use Taylor series expansion of the operator solution and make the short time (or short length of the medium) approximation to find the evolution of the quantum (operator) fields. This approach has been proposed by Tanaś [46] for approximate calculations of the higher-order field correlation functions in the process of nonlinear optical activity and later used by Kozierowski and Tanaś [21] for calculations of second order correlation function for the second-harmonic generation. Mandel [9] has used this approach to discuss squeezing and photon antibunching in harmonic generation. When doing calculations with operators it is crucial to keep track of the operator ordering and use the commutation relations to rearrange the ordering. This makes the calculations cumbersome and error-prone. The first calculations were performed by hand, but now we have computers that can do the job for us. The computer symbolic calculations of the subsequent terms in a series expansion have been performed by Bajer and Lisoněk [31] and Bajer and Peřina [32]. Bajer and Lisoněk [31] have written their own computer program for this purpose (about 3000 lines of code in Turbo Pascal). We want to show here how to do the same calculations with the freely available version of the computer program FORM [47] with only few lines of coding (see Appendix A).

The main idea of the approximate symbolic computations is based on the series expansion of any operator $\hat{O}(t)$ into a power series

$$\hat{O}(t) = \hat{O}(0) + \sum_{k=1}^{\infty} \frac{t^k}{k!} \frac{d^k}{dt^k} \hat{O}(t)\Big|_{t=0} \tag{90}$$

where the subsequent derivatives are obtained from the Heisenberg equations of motion

$$\frac{d}{dt}\hat{O} = \frac{1}{i\hbar}[\hat{O}, \hat{H}] \tag{91}$$

where $\hat{H}$ is the Hamiltonian. The higher derivatives are obtained recursively from (91), and the resulting expansion takes the form [31]

$$\hat{O}(t) = \hat{O}(0) + \sum_{k=1}^{\infty} \left(\frac{t}{i\hbar}\right)^k \frac{D_k}{k!} \tag{92}$$

where

$$D_k = [D_{k-1}, \hat{H}] = [\cdots[[\hat{O}(0), \hat{H}], \hat{H}], \ldots, \hat{H}] \tag{93}$$

is the kth-order commutator with $D_0 = \hat{O}(0)$.

Implementing the algorithm sketched above in the computer symbolic manipulation program FORM, as exemplified in Appendix A, and applying the method to the second-harmonic-generation (SHG) process, which is described by the interaction Hamiltonian $\hat{H}_I$ given by (55), one can easily calculate subsequent terms of the series (92). Restricting the calculations to the fourth-order terms, we get

$$\begin{aligned}\hat{a}(t) = \hat{a} &- 2i(\kappa t)\,\hat{a}^+\hat{b} - (\kappa t)^2\left(\hat{a}^+\hat{a}^2 - 2\hat{a}\hat{b}^+\hat{b}\right) \\ &- \frac{2}{3}\,i(\kappa t)^3\left(2\hat{a}^3\hat{b}^+ - 3\hat{a}^{+2}\hat{a}\hat{b} + 2\hat{a}^+\hat{b}^+\hat{b}^2 - \hat{a}^+\hat{b}\right) \\ &+ \frac{1}{6}(\kappa t)^4\left(5\hat{a}^{+2}\hat{a}^3 + 8\hat{a}^{+3}\hat{b}^2 - 28\hat{a}^+\hat{a}^2\hat{b}^+\hat{b} + 4\hat{a}\hat{b}^{+2}\hat{b}^2\right. \\ &\left. + \hat{a}^+\hat{a}^2 - 20\hat{a}\hat{b}^+\hat{b}\right) + \cdots \end{aligned} \tag{94}$$

$$\begin{aligned}\hat{b}(t) = \hat{b} &- i(\kappa t)\hat{a}^2 - (\kappa t)^2\left(2\hat{a}^+\hat{a}\hat{b} + \hat{b}\right) \\ &+ \frac{1}{3}\,i(\kappa t)^3\left(2\hat{a}^+\hat{a}^3 - 4\hat{a}^2\hat{b}^+\hat{b} + 4\hat{a}^{+2}\hat{b}^2 + \hat{a}^2\right) \\ &+ \frac{1}{6}(\kappa t)^4\left(2\hat{a}^{+2}\hat{a}^2\hat{b} - 4\hat{a}^4\hat{b}^+ - 16\hat{a}^+\hat{a}\hat{b}^+\hat{b}^2\right. \\ &\left. + 8\hat{a}^+\hat{a}\hat{b} - 8\hat{b}^+\hat{b}^2 + \hat{b}\right) + \cdots \end{aligned} \tag{95}$$

where the operators on the r.h.s. of equations (94) and (95) are at time $t = 0$. We can see that the terms that are of kth power in t contain the operator products that are of the $k + 1$ order as well as the products that are of the order $k - 1$,

$k-3,\ldots$. The latter products appeared as a result of application the bosonic commutation relations (4) for the operators of the two modes, and these terms represent purely quantum contributions that would not appear if the fields were classical. For classical fields, only the highest-order products survive. The quantum noise contributions appear in terms $\sim t^3$ and higher in the expansion (94) for the fundamental mode operators and in terms $\sim t^2$ and higher in the expansion (95) for the second harmonic mode operators. However, for the initial conditions representing the purely second-harmonic generation process, specifically, under the assumption that the harmonic mode is initially in the vacuum state such that $\hat{b}|0\rangle = 0$, we can drop all the terms containing operators $\hat{b}$ or $\hat{b}^+$ because they give zero due to the normal ordering of the operators. Assuming, moreover, that the pump beam is in a coherent state $|\alpha_0\rangle$ we find the following expansions for the mean values of the operators $\hat{a}(t)$ and $\hat{b}(t)$ [7]

$$\begin{aligned}\langle\hat{a}(t)\rangle &= \alpha_0\left[1-(\kappa t)^2|\alpha_0|^2+\frac{1}{6}(\kappa t)^4(5|\alpha_0|^4+|\alpha_0|^2)+\cdots\right]\\ \langle\hat{b}(t)\rangle &= -i\alpha_0^2\left[(\kappa t)-\frac{1}{3}(\kappa t)^3(2|\alpha_0|^2+1)+\cdots\right]\end{aligned} \tag{96}$$

or in the normalized variables (61) and scaled time (62), we have

$$\begin{aligned}u_a(\tau) &= u_a(0)e^{i\phi_a(0)}\left[1-\frac{\tau^2}{2}+\frac{5}{24}\tau^4\left(1+\frac{1}{5|\alpha_0|^2}\right)+\cdots\right]\\ u_b(\tau) &= u_a(0)^2e^{i(2\phi_a(0)-\pi/2)}\left[\tau-\frac{\tau^3}{3}\left(1+\frac{1}{2|\alpha_0|^2}\right)+\cdots\right]\end{aligned} \tag{97}$$

On neglecting the quantum noise terms, $\sim 1/|\alpha_0|^2$, one can easily recognize in (97) the first terms of the power series expansions of sech τ and tanh τ, which are the classical solutions. When $|\alpha_0|^2 \gg 1$, the quantum noise introduces only small corrections to the classical evolution of the field amplitudes. It is also seen that the phase of the second harmonic field is phase-locked so as to satisfy $\vartheta = 2\phi_a - \phi_b = \pi/2$.

We can thus expect from the short-time approximation that quantum noise does not significantly affect the classical solutions when the initial pump field is strong. We will return to this point later on, but now let us try to find the short-time solutions for the evolution of the quantum noise itself—let us take a look at the quadrature noise variances and the photon statistics. Using the operator solutions (94) and (95), one can find the solutions for the quadrature operators $\hat{Q}$ and $\hat{P}$ as well as for $\hat{Q}^2$ and $\hat{P}^2$. It is, however, more convenient to use the computer program to calculate the evolution of these quantities directly. Let us consider the purely SHG process, we drop the terms containing $\hat{b}$ and $\hat{b}^+$ after performing the normal ordering and take the expectation value in the coherent

state $|\alpha_0\rangle$ of the fundamental frequency mode, and in effect we arrive at

$$\begin{aligned}
\langle \hat{Q}_a^2(t)\rangle &= 1 + 2|\alpha_0|^2 + \alpha_0^2 + \alpha_0^{*2} \\
&\quad - (\kappa t)^2\left[4|\alpha_0|^4 + (2|\alpha_0|^2 + 1)(\alpha_0^2 + \alpha_0^{*2})\right] \\
&\quad + \frac{(\kappa t)^4}{6}\left[32|\alpha_0|^6 + 16|\alpha_0|^4 + \Big(16|\alpha_0|^4 \right. \\
&\quad \left. + 8|\alpha_0|^2 + 1\Big)(\alpha_0^{*2} + \alpha_0^2)\right] + \cdots \\
\langle \hat{P}_a^2(t)\rangle &= 1 + 2|\alpha_0|^2 - (\alpha_0^2 + \alpha_0^{*2}) \\
&\quad - (\kappa t)^2\left[4|\alpha_0|^4 - (2|\alpha_0|^2 + 1)(\alpha_0^2 + \alpha_0^{*2})\right] \\
&\quad + \frac{(\kappa t)^4}{6}\left[32|\alpha_0|^6 + 16|\alpha_0|^4 - \Big(16|\alpha_0|^4 \right. \\
&\quad \left. + 8|\alpha_0|^2 + 1\Big)(\alpha_0^{*2} + \alpha_0^2)\right] + \cdots \\
\langle \hat{Q}_b^2(t)\rangle &= 1 + (\kappa t)^2\Big(2|\alpha_0|^4 - (\alpha_0^4 + \alpha_0^{*4})\Big) - \frac{4}{3}(\kappa t)^4\left[2|\alpha_0|^6 \right. \\
&\quad \left. + |\alpha_0|^4 - (|\alpha_0|^2 + 1)(\alpha_0^{*4} + \alpha_0^4)\right] + \cdots \\
\langle \hat{P}_b^2(t)\rangle &= 1 + (\kappa t)^2\Big(2|\alpha_0|^4 + \alpha_0^4 + \alpha_0^{*4}\Big) - \frac{4}{3}(\kappa t)^4\left[2|\alpha_0|^6 \right. \\
&\quad \left. + |\alpha_0|^4 + (|\alpha_0|^2 + 1)(\alpha_0^{*4} + \alpha_0^4)\right] + \cdots
\end{aligned} \tag{98}$$

From equations (98) and (96) we obtain formulas for the field variances

$$\begin{aligned}
\langle [\Delta \hat{Q}_a(t)]^2\rangle &= 1 - (\kappa t)^2(\alpha_0^2 + \alpha_0^{*2}) \\
&\quad + (\kappa t)^4\left[2|\alpha_0|^4 + \left(|\alpha_0|^2 + \frac{1}{6}\right)(\alpha_0^2 + \alpha_0^{*2})\right] + \cdots \\
&= 1 - \tau^2 \cos 2\phi_a + \frac{1}{2}\tau^4\left[1 + \left(1 + \frac{1}{6N_a}\right)\cos 2\phi_a\right] + \cdots \\
\langle [\Delta \hat{P}_a(t)]^2\rangle &= 1 + (\kappa t)^2(\alpha_0^2 + \alpha_0^{*2}) \\
&\quad + (\kappa t)^4\left[2|\alpha_0|^4 - \left(|\alpha_0|^2 + \frac{1}{6}\right)(\alpha_0^2 + \alpha_0^{*2})\right] \\
&= 1 + \tau^2 \cos 2\phi_a + \frac{1}{2}\tau^4\left[1 - \left(1 + \frac{1}{6N_a}\right)\cos 2\phi_a\right] + \cdots \\
\langle [\Delta \hat{Q}_b(t)]^2\rangle &= 1 + \frac{2}{3}(\kappa t)^4(\alpha_0^4 + \alpha_0^{*4}) + \cdots = 1 + \frac{\tau^4}{3}\cos 4\phi_a + \cdots \\
\langle [\Delta \hat{P}_b(t)]^2\rangle &= 1 - \frac{2}{3}(\kappa t)^4(\alpha_0^4 + \alpha_0^{*4}) + \cdots = 1 - \frac{\tau^4}{3}\cos 4\phi_a + \cdots
\end{aligned} \tag{99}$$

It is easy to check, assuming $\phi_a = 0$, that the series expansion of the linearized solutions (88) agrees with (99) up to the leading terms, but in the higher-order terms there are already differences between the two solutions. Since the latter solutions are exact up to the fourth order, they show restricted applicability of the linearized solutions. We see that the quadratures $\langle[\Delta\hat{Q}_a(t)]^2\rangle$ and $\langle[\Delta\hat{P}_b(t)]^2\rangle$ become smaller than unity, showing squeezing, while the other two quadratures grow above unity.

The symbolic calculations using a computer allows for easy derivation of the approximate formulas for any operators for the two modes. Beside squeezing it is interesting to study the variance of the photon number operator for both modes in order to look for a possibility of obtaining the sub-Poissonian photon statistics in the process of second-harmonic generation. Let us calculate approximate formulas for the mean number of photons and the second order correlation function. Again, assuming initial conditions for pure second harmonic generation, $|\psi_0\rangle = |\alpha_0, 0\rangle$ with $|\alpha_0|^2 = N_a$, we have for the mean number of photons

$$\langle\hat{a}^+\hat{a}\rangle(t) = |\alpha_0|^2\left[1 - 2(\kappa t)^2|\alpha_0|^2 + \frac{4}{3}(\kappa t)^4|\alpha_0|^2(2|\alpha_0|^2 + 1) + \cdots\right]$$

$$\langle\hat{b}^+\hat{b}\rangle(t) = |\alpha_0|^4\left[(\kappa t)^2 - \frac{2}{3}(\kappa t)^4(2|\alpha_0|^2 + 1) + \cdots\right] \tag{100}$$

or in the scaled variables (61) and (62) Eqs. (100) take a very simple form

$$n_a(\tau) = u_a^2(\tau) = 1 - \tau^2 + \frac{2}{3}\tau^4\left(1 + \frac{1}{2N_a}\right) + \cdots$$

$$n_b(\tau) = u_b^2(\tau) = \tau^2 - \frac{2}{3}\tau^4\left(1 + \frac{1}{2N_a}\right) + \cdots \tag{101}$$

which explicitly shows the quantum noise contributions coming from the vacuum fluctuations.

The second order correlation functions can be obtained in the same manner giving

$$\langle\hat{a}^{+2}\hat{a}^2\rangle(t) = |\alpha_0|^4\Big[1 - 2(\kappa t)^2(2|\alpha_0|^2 + 1)$$
$$+ \frac{4}{3}(\kappa t)^4(7|\alpha_0|^4 + 8|\alpha_0|^2 + 1)\cdots\Big]$$

$$\langle\hat{b}^{+2}\hat{b}^2\rangle(t) = |\alpha_0|^8\left[(\kappa t)^4 - \frac{8}{3}(\kappa t)^6(|a_0|^2 + 1) + \cdots\right] \tag{102}$$

and combining equations (100) and (102) we obtain

$$\langle \hat{a}^{+2}\hat{a}^2\rangle(t) - \langle \hat{a}^{+}\hat{a}\rangle^2(t) = -2(\kappa t)^2|\alpha_0|^4 + \frac{4}{3}(\kappa t)^4|\alpha_0|^4(6|\alpha_0|^2 + 1) + \cdots$$
$$\langle \hat{b}^{+2}\hat{b}^2\rangle(t) - \langle \hat{b}^{+}\hat{b}\rangle^2(t) = -\frac{4}{3}(\kappa t)^6|\alpha_0|^8 + \cdots \tag{103}$$

The results (103), obtained first by Kozierowski and Tanaś [21], explain a very important property of the second harmonic generation, that is, the appearance of the sub-Poissonian photon statistics, which is an effect of quantum properties of the fields. The leading terms in (103) are negative, indicating, according to (18) and (19), that the photon statistics in both modes becomes sub-Poissonian at the initial stages of the evolution. The computer software now makes the calculations of this kind almost trivial and less error-prone. However, the results that we obtain in this way are just few terms of the power series expansion that properly describe the evolution of the system only at the initial stages of the evolution. The results can be improved by taking into account more and more terms of the expansion [31,32], but the long-time behavior cannot be predicted with such methods.

Some conclusions about the role of quantum noise in the long-time behavior of the solutions for the SHG process can be drawn by closer inspection of the operator equations of motion for the number of photon operators and their approximate solutions for the expectation values [38,48]. From the equations of motion (56) it is easy to derive the equations for the number of photons operators $\hat{N}_a = \hat{a}^{+}\hat{a}$ and $\hat{N}_b = \hat{b}^{+}\hat{b}$ in the form

$$-2\frac{d}{dt}\hat{N}_b = \frac{d}{dt}\hat{N}_a = -2i\kappa(\hat{a}^{+2}\hat{b} - \hat{a}^2\hat{b}^{+}) \tag{104}$$

and taking the derivative of the operator on the r.h.s. of Eq. (104) (again the symbolic manipulation program makes it easy), we get the second-order differential equation

$$\frac{d^2}{dt^2}\hat{N}_a = -2\frac{d}{dt}\hat{N}_b = -4\kappa^2[\hat{N}_a(\hat{N}_a - 1) - 4\hat{N}_a\hat{N}_b - 2\hat{N}_b] \tag{105}$$

and taking into account that $\hat{N}_a + 2\hat{N}_b = \hat{C}_0$ is a constant of motion, we find

$$\frac{d^2}{dt^2}(2\hat{N}_b) = 4\kappa^2[3(2\hat{N}_b)^2 - \hat{C}_0(1 + 4(2\hat{N}_b) + \hat{C}_0^2] \tag{106}$$

This second-order equation cannot be solved exactly because it contains operators $\hat{N}_b^2$ and $\hat{N}_b\hat{C}_0$, which, in turn, obey their own equations of motion

and we come into an infinite hierarchy of equations. However, if we neglect the correlations and take

$$\langle \hat{N}_b^2 \rangle = \langle \hat{N}_b \rangle^2 , \qquad \langle \hat{N}_b \hat{C}_0 \rangle = \langle \hat{N}_b \rangle \langle \hat{C}_0 \rangle \tag{107}$$

and introduce the normalized intensity $n_b = 2\langle \hat{N}_b \rangle / C_0$ and the scaled time $\tau = \sqrt{2C_0}\,\kappa t$ with $C_0 = \langle \hat{C}_0 \rangle$, we obtain the equation for the mean value of the normalized intensity n_b in the form

$$\frac{d^2}{d\tau^2} n_b = 2\left[3n_b^2 - 4n_b + 1 - \frac{1}{C_0}\right] \tag{108}$$

This is the second-order differential equation, which reminds us of the equation for a particle moving under the action of a force, and the force can be derived from a potential. There is a quantity that is conserved during this motion, and we can write

$$\frac{d}{d\tau}\left[\frac{1}{2}\left(\frac{dn_b}{d\tau}\right)^2 - 2n_b[(1-n_b)^2 - \epsilon']\right] = 0 \tag{109}$$

where $\epsilon' = 1/C_0$ is the term representing the quantum noise contribution (it comes from application of the commutation rules to the field operators). The quantity in the square brackets can be considered as the total energy of a "particle" at position n_b, with the kinetic energy $\frac{1}{2}(dn_b/d\tau)^2$ and the potential energy $V = -2n_b[(1-n_b)^2 - \epsilon']$. The potential energy is shown in Fig. 4. The potential represents a well in which the particle will oscillate exhibiting fully periodic behavior. From Eq. (109) we get

$$\frac{dn_b}{d\tau} = 2\sqrt{n_b(1-n_b)^2 - n_b\epsilon'} \tag{110}$$

Comparing Eq. (110) with Eq. (66), we find that both equations have extra terms (the ϵ or ϵ' terms) which make the solutions oscillatory, but the physical reason for oscillations is different in both cases. In Eq. (66) different from zero ϵ comes from the nonzero initial value of the second-harmonic mode intensity, while in Eq. (110) the nonzero value of ϵ' comes from the quantum noise. We can interpret this fact in the following way. It is the spontaneous emission of photons, or vacuum fluctuations of the second harmonic mode, that contribute to the nonzero value of the initial intensity of the second harmonic mode and lead to the periodic evolution. This means that the very small quantum fluctuations can cause macroscopic effects, such as quantum-noise-induced macroscopic revivals [38], in the nonlinear process of second-harmonic generation.

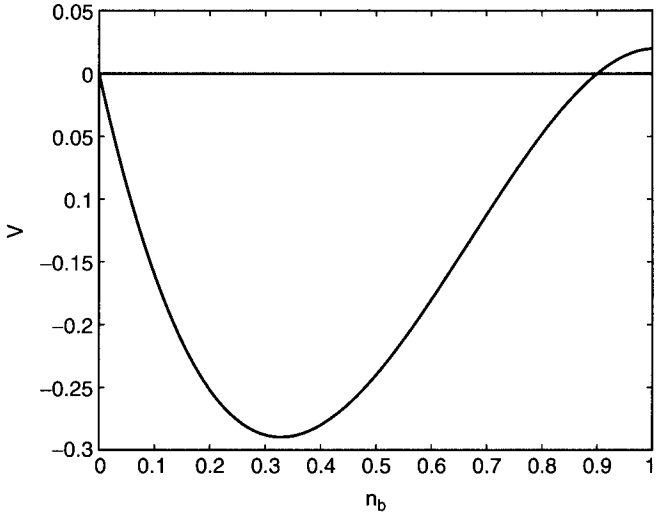

Figure 4. Plot of the pseudopotential curve for $\epsilon' = 0.01$.

A procedure similar to that used to solve equation (66) can be applied to solve equation (110). Again, the solution is given by the Jacobi elliptic functions. The third-order polynomial under the square root on the r.h.s. of (110) has the roots

$$n_{b1} = 0\,, \qquad n_{b2} = 1 - \sqrt{\epsilon'}\,, \qquad n_{b3} = 1 + \sqrt{\epsilon'} \tag{111}$$

and the solution has the form

$$n_b(\tau) = \sqrt{1 - \sqrt{\epsilon'}}\ \mathrm{sn}^2\left(\sqrt{1 + \sqrt{\epsilon'}}\,\tau \,|\, k^2\right) \tag{112}$$

where

$$k^2 = \frac{1 - \sqrt{\epsilon'}}{1 + \sqrt{\epsilon'}} \tag{113}$$

The results have been recently obtained by Olsen et al. [38], and they show that even for almost vanishingly small ϵ', which is inversely proportional to the initial mean value of the number of the pump mode photons, usually very large, the quantum fluctuations have huge macroscopic effect on the system dynamics. It is evident that the quantum noise, which is always present, is responsible for the oscillations between the two regimes of second-harmonic generation and downconversion. The period of oscillation is becoming infinite as ϵ' vanishes.

The solution (112) is fully periodic, but it does not allow for the complete transfer of energy from the fundamental to the second harmonic mode. The maximum that can be achieved by u_b is equal to $\sqrt{1-\sqrt{\epsilon'}}$. We have to remember, moreover, that the solution (112) has been obtained with the decorrelation (107), and it is only an approximate solution.

D. Numerical Methods

When analytical solutions are not known and the approximate analytical methods give results of limited applicability, the numerical methods may be a solution. Let us first discuss a method based on the diagonalization of the second-harmonic Hamiltonian [48,49]. As we have already said, the two parts of the Hamiltonian $\hat{H}_0$ and $\hat{H}_I$ given by (55), commute with each other, so they are both constants of motion. The $\hat{H}_0$ determines the total energy stored in both modes, which is conserved by the interaction $\hat{H}_I$. This means that we can factor the quantum evolution operator

$$\exp\left(\frac{-i\hat{H}t}{\hbar}\right) = \exp\left(\frac{-i\hat{H}_0 t}{\hbar}\right)\exp\left(\frac{-i\hat{H}_I t}{\hbar}\right) \tag{114}$$

If the Fock state basis is used to describe the field state, we find, for the initial state $|n,0\rangle = |n\rangle|0\rangle$ with n photons in the fundamental mode and zero photons in the second harmonic mode, that the Hamiltonian $\hat{H}_0$ splits the Hilbert space into orthogonal sectors. Since $\hat{H}_0$ is a constant of motion, we have for a given number of photons n the relation

$$\langle \hat{a}^+\hat{a}\rangle + 2\langle \hat{b}^+\hat{b}\rangle = n \tag{115}$$

which implies that the creation of k photons of the second-harmonic mode requires annihilation of $2k$ photons of the fundamental mode. Thus, for given n, we can introduce the states

$$|\psi_k^{(n)}\rangle = |n-2k,k\rangle\,, \qquad k = 0,1,\cdots,\left[\frac{n}{2}\right] \tag{116}$$

where $[n/2]$ means the integer part of $n/2$, which form a complete basis of states of the field in the sector with given n. We have

$$\langle \psi_{k'}^{(n')}|\psi_k^{(n)}\rangle = \delta_{nn'}\delta_{kk'} \tag{117}$$

which means that the subspace with given n has $[n/2]+1$ orthogonal states. In such a basis the interaction Hamiltonian $\hat{H}_I$ has the following nonzero matrix elements

$$\begin{aligned}\langle \psi_{k+1}^{(n)}|\hat{H}_I|\psi_k^{(n)}\rangle &= \langle \psi_k^{(n)}|\hat{H}_I|\psi_{k+1}^{(n)}\rangle = (\hat{H}_I)_{k+1,k}^{(n)} = (\hat{H}_I)_{k,k+1}^{(n)} \\ &= \hbar\kappa\sqrt{(k+1)(n-2k)(n-2k-1)}\end{aligned} \tag{118}$$

which form a symmetric matrix of dimension $([n/2]+1)\times([n/2]+1)$ with real nonzero elements (we assume that κ is real) that are located on the two diagonals immediately above and below the principal diagonal. Such a matrix can easily be diagonalized numerically [49]. To find the quantum state evolution, we need the matrix elements of the evolution operator. Since the evolution due to the Hamiltonian $\hat{H}_0$ at each sector of the Hilbert space with given n introduces only a constant phase factor $\exp(-in\omega t)$, we will drop this factor in our calculations and calculate the state at time t according to the formula

$$|\psi(t)\rangle = \exp\left(\frac{-i\hat{H}_I t}{\hbar}\right)|\psi(0)\rangle \tag{119}$$

where $|\psi(0)\rangle$ is the initial state of the field. In each subspace of the Hilbert space we can calculate the matrix elements of the evolution operator

$$c_{n,k}(t) = \langle\psi_k^{(n)}|\exp\left(\frac{-i\hat{H}_I t}{\hbar}\right)|\psi_0^{(n)}\rangle \tag{120}$$

by diagonalizing the Hamiltonian matrix (118). If the matrix U is the unitary matrix that diagonalizes the interaction Hamiltonian matrix (118)

$$U^{-1}\hat{H}_I^{(n)}U = \hbar\kappa\,\mathrm{diag}\left(\lambda_0, \lambda_1, \ldots, \lambda_{[n/2]}\right) \tag{121}$$

then the coefficients $c_{n,k}(t)$ can be written as

$$c_{n,k}(t) = \sum_{j=0}^{[n/2]} e^{-i\kappa t\lambda_j} U_{kj}U_{0j}^* \tag{122}$$

where λ_j are the eigenvalues of the interaction Hamiltonian in units of $\hbar\kappa$. Of course, the matrix U as well as the eigenvalues λ_j are defined for given n and should have an additional index n, which we have omitted to shorten the notation. Moreover, for real κ the interaction Hamiltonian matrix is real, and the transformation matrix U is a real orthogonal matrix, so the star can also be dropped.

The numerical diagonalization procedure gives the eigenvalues λ_j as well as the elements of the matrix U, and the coefficients $c_{n,k}(t)$ can thus be calculated according to (122). It is worthwhile to note, however, that because of the symmetry of the Hamiltonian, the eigenvalues λ_j are distributed symmetrically with respect to zero, with one eigenvalue equal to zero if there is an odd number of them. When the eigenvalues are numbered from the lowest to the highest

value, there is an additional relation

$$U_{kj}U_{0j} = (-1)^k U_{k,[n/2]-j}U_{0,[n/2]-j} \tag{123}$$

which makes the coefficients $c_{n,k}(t)$ either real (k even) or imaginary (k odd). This property of the coefficients $c_{n,k}(t)$ is very important and allows in some cases to get exact analytical results.

Knowing the coefficients $c_{n,k}(t)$ the resulting state of the field (119) in the particular sector can be written, for the initial state $|n,0\rangle$, as

$$|\psi^{(n)}(t)\rangle = \sum_{k=0}^{[n/2]} c_{n,k}(t)|\psi_k^{(n)}\rangle \tag{124}$$

The typical initial conditions for the second-harmonic generation are a coherent state of the fundamental mode and the vacuum of the second-harmonic mode. The initial state of the field can thus be written as

$$|\psi(0)\rangle = \sum_{n=0}^{\infty} \mathrm{e}^{in\phi_a} b_n |n,0\rangle \tag{125}$$

where

$$b_n = \exp\left(\frac{-N_a}{2}\right)\frac{N_a^{n/2}}{\sqrt{n!}} \tag{126}$$

is a Poissonian weighting factor of the coherent state $|\alpha_0\rangle$ represented as a superposition of the number states, $N_a = |\alpha_0|^2$ is the mean number of photons, and ϕ_a is the phase of the coherent state — $\alpha_0 = \sqrt{N_a}\exp(i\phi_a)$. With these initial conditions the resulting state of the field (119) takes the form

$$\begin{aligned} |\psi(t)\rangle &= \sum_{n=0}^{\infty} e^{in\phi_a} b_n |\psi^{(n)}(t)\rangle \\ &= \sum_{n=0}^{\infty} e^{in\phi_a} b_n \sum_{k=0}^{[n/2]} c_{n,k}(t)|n-2k,k\rangle \end{aligned} \tag{127}$$

Equation (127) describing the evolution of the system is our starting point for further discussion of the second-harmonic generation. If the initial state of the fundamental mode is not a coherent state but has a decomposition into a number states of the form (125) with different b_n, equation (127) is still valid when corresponding b_n are taken. It is true, for example, for the initially squeezed state of the fundamental mode.

It is interesting to consider one particular initial state of the field in which there are only two photons at the fundamental mode and no photons in the second-harmonic mode: $|2,0\rangle$. With this initial state the only state that can be created in the process is the state $|0,1\rangle$ with one photon in the second-harmonic mode and zero photons in the fundamental mode. Next, the second-harmonic photon can be downconverted into two photons of the fundamental mode, and we observe fully periodic evolution. The evolution is thus restricted to the two-dimensional subspace $\{|2,0\rangle, |0,1\rangle\}$. The Hamiltonian matrix in this subspace has the form

$$H_I = \hbar\kappa \begin{pmatrix} 0 & \sqrt{2} \\ \sqrt{2} & 0 \end{pmatrix} \tag{128}$$

the diagonalizing matrix U has the form

$$U = \frac{1}{\sqrt{2}} \begin{pmatrix} 1 & 1 \\ -1 & 1 \end{pmatrix}, \qquad U^{-1} = \frac{1}{\sqrt{2}} \begin{pmatrix} 1 & -1 \\ 1 & 1 \end{pmatrix} \tag{129}$$

and the two eigenvalues are $\lambda_0 = -\sqrt{2}$ and $\lambda_1 = \sqrt{2}$. We have two coefficients $c_{n,k}(t)$

$$c_{2,0}(t) = \cos(\sqrt{2}\,\kappa t), \qquad c_{2,1}(t) = -i\sin(\sqrt{2}\,\kappa t) \tag{130}$$

and the resulting state has the form

$$|\psi^{(2)}(t)\rangle = \cos(\sqrt{2}\,\kappa t)|2,0\rangle - i\sin(\sqrt{2}\,\kappa t)|0,1\rangle \tag{131}$$

The mean numbers of photons in the state (131) are given by

$$\langle \hat{a}^+\hat{a}\rangle(t) = 2\cos^2(\sqrt{2}\,\kappa t), \qquad \langle \hat{b}^+\hat{b}\rangle(t) = \sin^2(\sqrt{2}\,\kappa t) \tag{132}$$

which are exact analytical formulas for these particular initial conditions. We also have

$$\begin{aligned} \langle \hat{a}^{+2}\hat{a}^2\rangle - \langle \hat{a}^+\hat{a}\rangle^2 &= -2\cos^2\sqrt{2}\,\kappa t(2\cos^2\sqrt{2}\,\kappa t - 1) \\ \langle \hat{b}^{+2}\hat{b}^2\rangle - \langle \hat{b}^+\hat{b}\rangle^2 &= -\sin^4\sqrt{2}\,\kappa t \end{aligned} \tag{133}$$

From the definition (19) of the Mandel q parameter and Eq. (133) we immediately find that

$$q_a = 1 - 2\cos^2\sqrt{2}\,\kappa t, \qquad q_b = -\sin^2\sqrt{2}\,\kappa t \tag{134}$$

which shows that initially the fundamental mode has $q_a = -1$ denoting the sub-Poissonian statistics of the initial Fock state with two photons and the second harmonic mode initially has $q_b = 0$, as it should be for the vacuum state. At later times, however, the fundamental mode becomes super-Poissonian while the second-harmonic mode becomes sub-Poissonian. This simple example shows that even in the case of the evolution that is restricted to the two-dimensional subspace, there are essential changes in photon statistics.

Generally, the second-harmonic generation is described by the quantum state (127) and we use this state in our further calculations. Classical solutions discussed earlier, $u_a(\tau) = \operatorname{sech}\tau$ and $u_b(\tau) = \tanh\tau$, indicated that the amplitudes of the two modes are monotonic functions of time and that eventually all the energy from the fundamental mode will be transferred into the second-harmonic mode, assuming that there was no second-harmonic signal initially. It is well known [20,48], however, that the quantum solution has oscillatory character and does not allow for the complete power transfer. Using the state (127) we find that the mean photon numbers evolve in time according to the formulas

$$\langle \hat{N}_a(t)\rangle = \langle \psi(t)|\hat{a}^+\hat{a}|\psi(t)\rangle = \sum_{n=0}^{\infty} b_n^2 \sum_{k=0}^{[n/2]} (n-2k)|c_{n,k}(t)|^2$$

$$\langle \hat{N}_b(t)\rangle = \langle \psi(t)|\hat{b}^+\hat{b}|\psi(t)\rangle = \sum_{n=0}^{\infty} b_n^2 \sum_{k=0}^{[n/2]} k|c_{n,k}(t)|^2 \tag{135}$$

Because of the Poissonian factors, which are peaked at N_a, the summation over n can be performed numerically if N_a is not too great. On the other hand, some features of the classical solutions can be expected for $N_a \gg 1$. To evaluate numerically formulas (135) we use the computer program quoted in the Appendix B, which can be run using the freely available software OCTAVE [50] or the commercial software MATLAB [51]. The results are illustrated in Fig. 5. In Fig. 5a we have plotted the normalized second-harmonic intensity $n_b = 2\langle \hat{N}_b\rangle/N_a$, where N_a is the initial mean number of photons of the coherent state of the fundamental mode, against the scaled time τ for the initially coherent state with the mean number of photons equal to 2 (solid line) and compared it with the corresponding intensity obtained for the initial state of the fundamental mode being the Fock state with two photons [Eq. (132)]. In the latter case we see the perfectly periodic behavior with complete transfer of energy between the fundamental and second-harmonic modes. In the case of coherent state with the mean number of photons being the same as for the Fock state we already see the distorted oscillations, and the transfer of power is not complete. In Fig. 5b we have presented the results for initially coherent state of the fundamental mode with the mean number of photons satisfying the inequal-

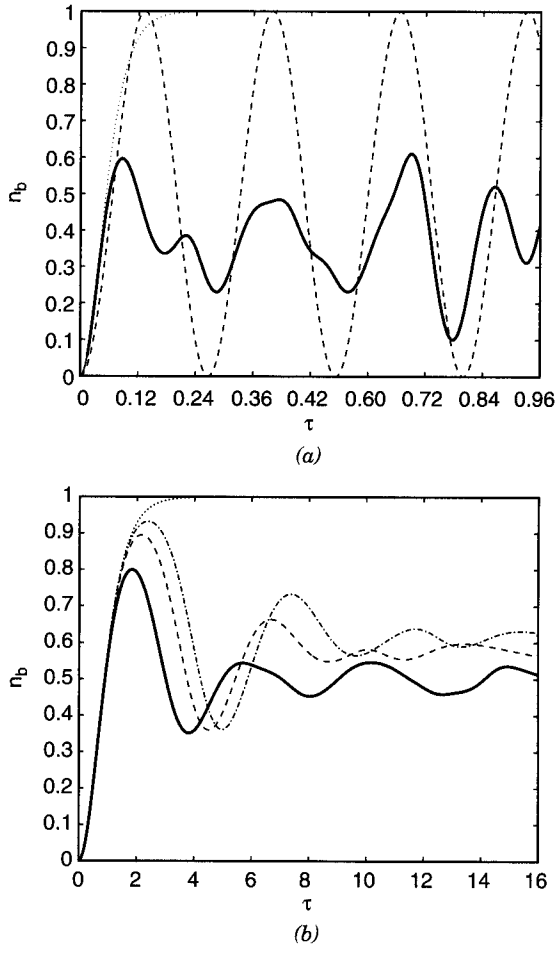

Figure 5. Intensity of the second-harmonic: (a) initial coherent state with $N_a = 2$ (solid line) and initial number state with two photons (dashed line); (b) initial coherent state with $N_a = 10$ (solid line), $N_a = 40$ (dashed line), and $N_a = 100$ (dashed–dotted line). Dotted line marks the classical solution.

ity $N_a \gg 1$. The curves are plotted for $N_a = 10$ (solid line), $N_a = 40$ (dashed line), and $N_a = 100$ (dashed-dotted line). For reference, with the dotted line the classical solution is marked on both figures. The solutions are oscillatory but the oscillations are damped rather quickly when the pump mode is strong. The higher is the intensity of the pump mode, the longer the solution sticks to the classical solution before the process is reversed from the second-harmonic

generation into the downconversion. The maximum reached by the second harmonic intensity increases, as the intensity of the pump mode increases, giving better efficiency of conversion of the fundamental mode field into the second harmonic. This tendency is clearly seen from Fig. 5b.

At this point it is interesting and worthwhile to compare the solution (112) that predicted fully periodic behavior resulting from the quantum noise with the fully quantum calculations performed in this section. In Fig. 6 we present both solutions for the initial mean number of photons $N_a = 100$, which gives $\epsilon' = 0.01$. Both solutions are almost identical up to the first maximum, but subsequent maxima are substantially damped with respect to the approximate solution. The approximate solution correctly predicts the transition from the second harmonic regime to the downconversion regime, which is the physical reason for starting oscillations. The quantum noise really induces macroscopic revivals, but subsequent maxima are smaller and smaller and the second harmonic intensity asymptotically approaches a certain value. Without quantum fluctuations the solution is a monotonic function as shown in the figure by the dotted curve. The quantum noise is necessary to trigger the macroscopic changes in the intensity of the second-harmonic mode.

Now, we can proceed further and ask the question about the evolution of the quantum fluctuations. We have already seen that there are essential changes in

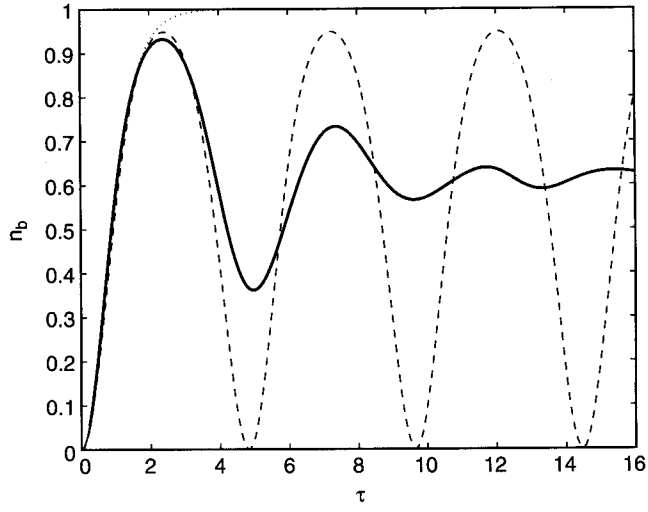

Figure 6. Comparison of the fully quantum numerical solution (solid line) and the approximate solution (112) (dashed line) for the initial mean number of photons $N_a = 100(\epsilon' = 0.01)$. Classical solution is marked by dotted curve.

the photon statistics when the evolution is restricted to the two-state subspace. Even in this simple case the fundamental mode evolved from the sub- to super-Poissonian photon statistics. The numerical method presented above is suitable for answering questions about photon statistics and squeezing equally well as the question about the mean intensity. To calculate the mean value of the square of the photon number operator for the fundamental mode, it is as simple as replacing $n - 2k$ by $(n - 2k)^2$ in (135), or replacing k by k^2 in order to calculate the mean value of the square of the photon number operator for the second-harmonic mode. All the rest is up to the computer. Let us calculate the Mandel q parameter as defined by (19). In Fig. 7 we have presented the results of the numerical calculations for the Mandel q parameters for both fundamental (Fig. 7a) and second harmonic (Fig. 7b) modes. Both modes exhibit sub-Poissonian photon statistics (negative values of the q parameter) at the initial stages of the evolution, but for long times the statistics becomes super-Poissonian. The sub-Poissonian statistics at initial stages of the evolution is in agreement with the short time approximation presented in Eq. (103).

In Fig. 8 we have plotted the quadrature variances for the two modes and compared them to their counterparts obtained from the linearized noise equations. In Fig. 8a we see the two squeezed quadratures, $\langle[\Delta Q_a]^2\rangle$ and $\langle[\Delta P_b]^2\rangle$, calculated numerically for the mean number of photons of the pump mode $N_a = 10$, and their counterparts obtained from the linearized theory, that is, plotted from the formulas (88). In Fig. 8b the nonsqueezed quadratures $\langle[\Delta P_a]^2\rangle$ and $\langle[\Delta Q_b]^2\rangle$ are compared. It is evident from the figures that, as one could expect, the linearized theory has only limited range of applicability. The linearized results are in good agreement with the exact numerical results roughly up to the scaled time $\tau \simeq 1$. The long-time evolution ($\tau > 1$) of the quadrature variances is principally different from their linearized approximation counterparts because the linearization fails to predict the quantum noise induced revival in the evolution. It is also clear from Fig. 8a that the degree of squeezing that can really be obtained is much smaller than that predicted from the linearized theory. The long time behavior of the quadrature variances is presented in Fig. 9 where the same quadratures are plotted as in Fig. 8 but for longer time τ showing irregular oscillations of the quantum noise with a general tendency for that noise to increase and we should not expect squeezing in the long time-limit. The reduction of the quantum noise below the vacuum level is thus a property that in second-harmonic generation appears at the beginning of the evolution and never reappears again.

Since $\hat{H}_0$ is a constant of motion, $\hat{H}_0^2$ is also a constant of motion, which gives, for the fluctuations of $\hat{H}_0$, the relation

$$\langle[\Delta\hat{H}_0]^2\rangle = \langle\hat{H}_0^2\rangle = \langle\hat{H}_0\rangle^2 = N_a(\hbar\omega)^2 \tag{136}$$

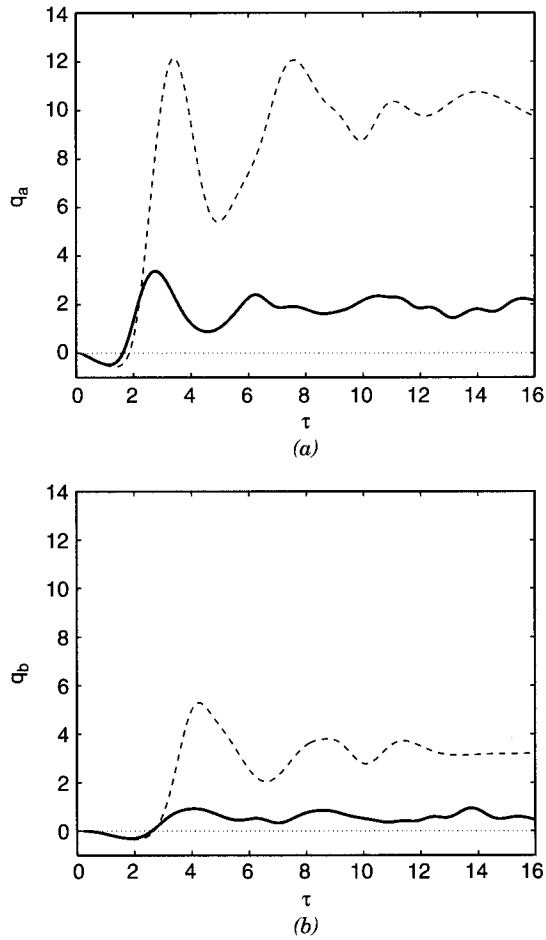

Figure 7. The Mandel q parameter for the (a) fundamental mode and; (b) second-harmonic mode. The mean number of photons is $N_a = 10$ (solid lines) and $N_a = 40$ (dashed lines).

which can be rewritten as

$$\langle[\Delta\hat{N}_a]^2\rangle + 4\langle[\Delta\hat{N}_b]^2\rangle + 4\langle\Delta\hat{N}_a\Delta\hat{N}_b\rangle = N_a \tag{137}$$

Formula (137) establishes the relation between the fluctuations of the individual-mode photon numbers and the intermode photon-number correlation. All the quantities on the left hand side (l.h.s.) of Eq. (137) can be calculated

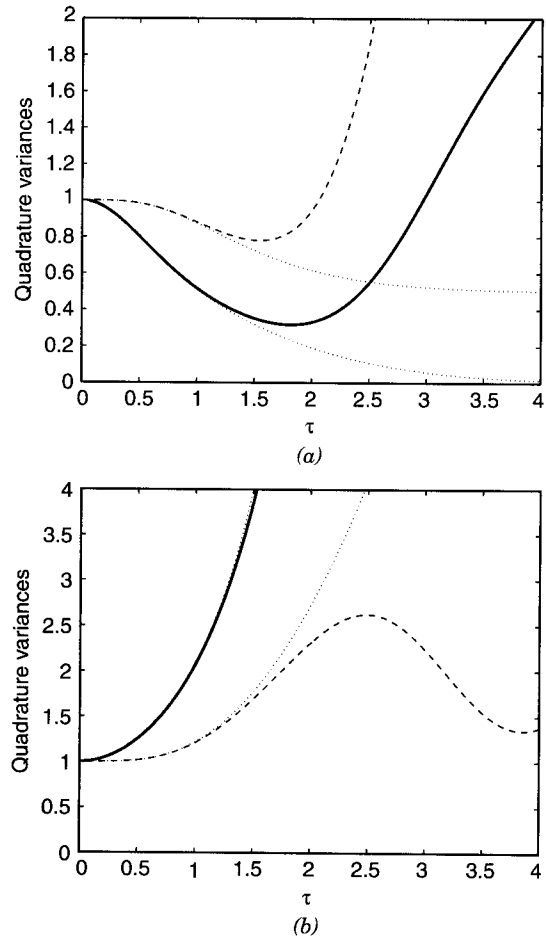

Figure 8. The quadrature variances: (a) squeezed variances $\langle[\Delta Q_a]^2\rangle$ (solid line) and $\langle[\Delta P_b]^2\rangle$ (dashed line) (b) nonsqueezed variances $\langle[\Delta P_a]^2\rangle$ (solid line) and $\langle[\Delta Q_b]^2\rangle$ (dashed line) for $N_a = 10$. The dotted lines are the linearized solutions.

numerically starting with the state (127), and formula (137) can serve as a test of numerical precision. The value of N_a sets the level of fluctuations for an initially coherent state with the mean number of photons N_a. In Fig. 10 we have visualized the evolution of the correlations between the photon-number fluctuations (normalized) $4\langle\Delta\hat{N}_a\Delta\hat{N}_b\rangle/N_a$ of the two modes. The two photon noises are negatively correlated. This negative correlation of photon fluctuations compensates for the large increase of the photon number variances in each

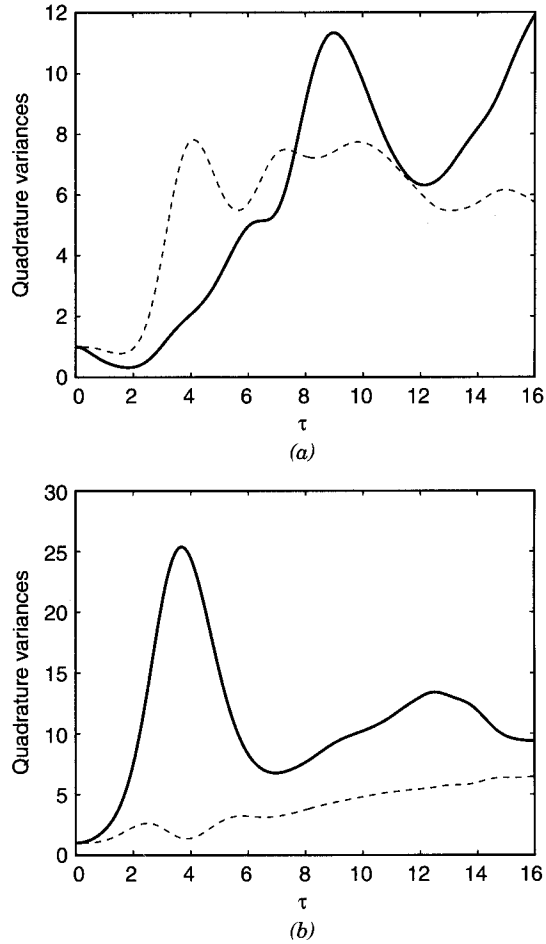

Figure 9. Same quadratures as in Fig. 8 but for longer time τ.

mode, which is clearly visible from Fig. 7. Thus the super-Poissonian photon statistics is related with the appearance of strong negative correlations between the photon-number fluctuations. The peak in the Mandel q parameter, indicating highly super-Poissonian photon statistics, is, on the other hand, related to the minimum of the quadrature variance, that is, it is related to the maximum of squeezing. This shows that quantum fluctuations of various physical quantities are related to each other, but this relation is not necessarily simple.

The statistical properties of the quantum fields are well characterized by the quasiprobability distribution functions defined in the Section II. Let us consider

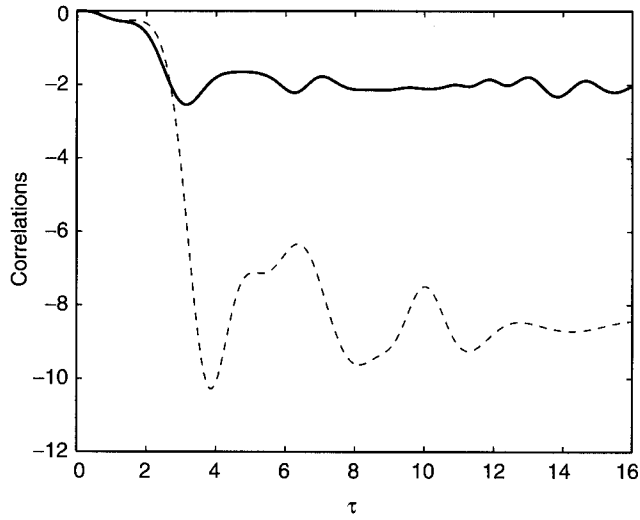

Figure 10. Correlations $4\langle\Delta\hat{N}_a\Delta\hat{N}_b\rangle/N_a$ between the photon-number fluctuations in the two modes for $N_a = 10$ (solid line) and $N_a = 40$ (dashed line). Compare to Fig. 7.

the Husimi Q function as defined by (28) for the fundamental mode. To find this function, we start with the more general function for the two-mode field

$$Q(\alpha,\beta) = \frac{1}{\pi^2}|\langle\alpha,\beta|\psi(t)\rangle|^2 \tag{138}$$

where $|\psi(t)\rangle$ is as given by (127). By integrating the function $Q(\alpha,\beta)$ over $d^2\beta$, we obtain the function $Q(\alpha)$ for the fundamental mode. We find

$$Q(\alpha,\beta) = \frac{1}{\pi^2}e^{-(|\alpha|^2+|\beta|^2)}\left|\sum_{n=0}^{\infty}e^{in\phi_a}b_n\sum_{k=0}^{[n/2]}\frac{(\alpha^*)^{n-2k}(\beta^*)^k}{\sqrt{(n-2k)!k!}}c_{n,k}(t)\right|^2 \tag{139}$$

and after integrating over $d^2\beta$ we get

$$\begin{aligned}Q(\alpha) = \frac{1}{\pi}e^{-|\alpha|^2}\Bigg\{&\sum_{n=0}^{\infty}|b_n|^2|\alpha|^{2n}\sum_{k=0}^{[n/2]}\frac{|\alpha|^{-4k}|c_{nk}(t)|^2}{(n-2k)!}\\&+2\mathrm{Re}\sum_{n=1}^{\infty}\sum_{n'=0}^{n-1}e^{i(n-n')\phi_a}b_nb_{n'}(\alpha^*)^n\alpha^{n'}\\&\times\sum_{k=0}^{[n'/2]}\frac{|\alpha|^{-4k}c_{n,k}(t)c^*_{n',k}(t)}{\sqrt{(n-2k)!(n'-2k)!}}\Bigg\}\end{aligned} \tag{140}$$

In a similar way, integrating (139) over $d^2\alpha$ we obtain the Q function for the second-harmonic mode, which has the form

$$Q(\beta) = \frac{1}{\pi} e^{-|\beta|^2} \left\{ \sum_{n=0}^{\infty} \sum_{n'=0}^{\infty} e^{i(n-n')\phi_a} b_n b_{n'} \right.$$
$$\left. \times \sum_{k=0}^{[n/2]} \sum_{k'=0}^{[n'/2]} \frac{(\beta^*)^k \beta^{k'}}{\sqrt{k!k'!}} c_{n,k}(t) c^*_{n',k'}(t) \delta_{n-2k,n'-2k'} \right\} \tag{141}$$

The two functions can be evaluated numerically for a not-too-large mean number of photons N_a. In Fig. 11 we have shown the contour plots of the Q function for the fundamental mode (Fig. 11a) and the second-harmonic mode (Fig. 11b) for the initial mean number of photons of the fundamental mode $N_a = 10$. It is seen that the centroid of the distribution, in case of the fundamental mode, moves to the left along the Re α axis showing squeezing along this axis at initial stages of the evolution, and next it becomes a two-peak structure first noticed by Nikitin and Masalov [24]. Nikitin and Masalov [24] suggested that the two peaks appearing in the Q function indicated a macroscopic superposition of quantum states. In case of the second harmonic mode the Q function starts with the peak localized at the origin (initial vacuum state) and moves along the Im β axis undergoing deformation during the evolution. Motion of the centroid of the distribution along the Im β axis confirms again our earlier prediction that the phases of the two fields exhibit a shift by $\pi/2$. The Q function is one of the quasiprobalility distributions that describe quantum statistical properties of the field. It has advantage that it is always positive, so it can be treated in the way as the classical probability distributions are treated, but it also has disadvantages; for example, it does not lead to correct marginal distributions. In this context the Wigner function is more appropriate, but the Wigner function can take negative values, which precludes its treatment as classical probability distribution. In many cases, however, the Wigner function is very useful. All the quasidistribution functions take into account the fact that quantum fields are operator fields and are represented by noncommuting operators, which unavoidably introduce quantum noise. The different quasidistributions are related to different orderings of the field operators. The Q function is associated with the antinormal ordering of the operators.

As we have already seen, quantum noise changes the character of the evolution of the field in the second-harmonic generation by making it periodic. But periodic behavior is also seen for classical solution if we assume that there is a small classical signal of the second harmonic mode when the evolution starts. One can thus say that the quantum noise, or spontaneously emitted photons, play a role of the classical signal that makes the evolution periodic.

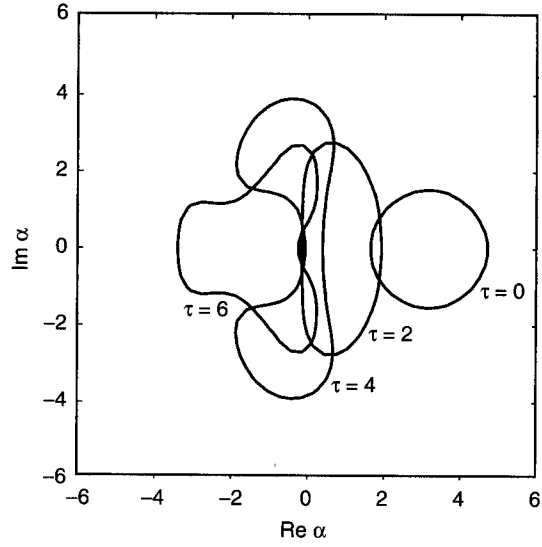

(a)

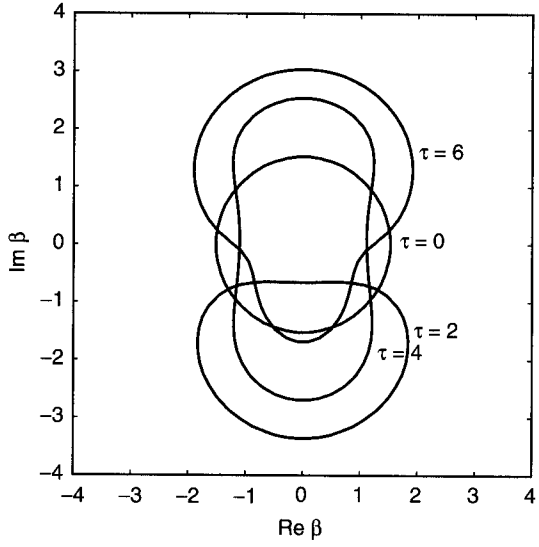

(b)

Figure 11. Contour plots for the Q function: (a) fundamental mode and (b) second-harmonic mode, for the mean number of photons $N_a = 10$. Contours are taken at 0.1 of the maximum.

This also prompts us a way to simulate the quantum noise by introducing randomly chosen initial values. We can use deterministic classical equation of motion to describe the evolution of the fields, but the initial conditions are chosen at random. Let us assume that $\alpha = \alpha_0 + \Delta\alpha$, $\beta = \beta_0 + \Delta\beta$, where α_0 and β_0 are the mean values of the initial amplitudes and $\Delta\alpha = \Delta x_a + i\Delta y_a$, $\Delta\beta = \Delta x_b + i\Delta y_b$ are the fluctuations of the two fields, where Δx_a, Δy_a, Δx_b, Δy_b being the independent real Gaussian processes with identical variances $\overline{\Delta x_a^2} = \overline{\Delta y_a^2} = \overline{\Delta x_b^2} = \overline{\Delta y_b^2} = \frac{1}{4}$, where we have denoted the classical averaging by the overline (vinculum). With these assumptions we find that the variances of the quadrature components $\hat{Q}$ and $\hat{P}$ of the fields, which for the vacuum state are equal to unity, can be expressed by the variances of these classical random variables $\langle[\Delta\hat{Q}_a]^2\rangle = 2(\overline{\Delta x_a^2} + \overline{\Delta y_a^2}) = 1$, and so on. Now, starting with the Gaussian distribution of the initial values of the field amplitudes, we can simulate some quantum properties of the fields using classical trajectories. It is interesting to compare the results obtained using the method of classical trajectories to the quantum results for the Q function. This kind of comparison has been done for second-harmonic process by Nikitin and Masalov [24]. Since it is really impressive to see how good the quantum Q function contours are reproduced by a cloud of points that undergone classical evolution starting from the initial conditions described by the Gaussian distribution, we show in Fig. 12 clouds of 1000 points for the same values of the evolution time as in Fig. 11 for $N_a = 10$. Why is the Q function reproduced so well with the classical trajectories? The Q function is a representative of a whole class of the quasidistribution functions. Generally, the s-parametrized quasiprobability distribution for a coherent state, defined by (30), is given by

$$\mathscr{W}^{(s)}(\alpha) = \frac{1}{\pi}\frac{2}{1-s}\exp\left(-\frac{2}{1-s}|\alpha - \alpha_0|^2\right) \tag{142}$$

which, for $s < 1$, is a Gaussian distribution. For $s = 1$, the distribution becomes the Dirac delta function, for $s = 0$ it is the Wigner function, and for $s = -1$, we have the Q function. The distribution (142) becomes narrower as s increases approaching unity. The Q function is the broadest distribution, but all of them for $s < 1$ are just Gaussians with various variances. In terms of classical description of the field noise, the most suitable function is the Wigner function [52], for which the variance of the Gaussian distribution is equal to $\frac{1}{4}$. The Q function is broader, with the variance equal to $\frac{1}{2}$, but because the state of the field has a large coherent component, the two functions are very similar in shape and the Q function is usually easier to calculate. For the nontrivial quantum states, the Wigner function can take negative values, and then it is difficult to simulate properties of such states by classical stochastic variables

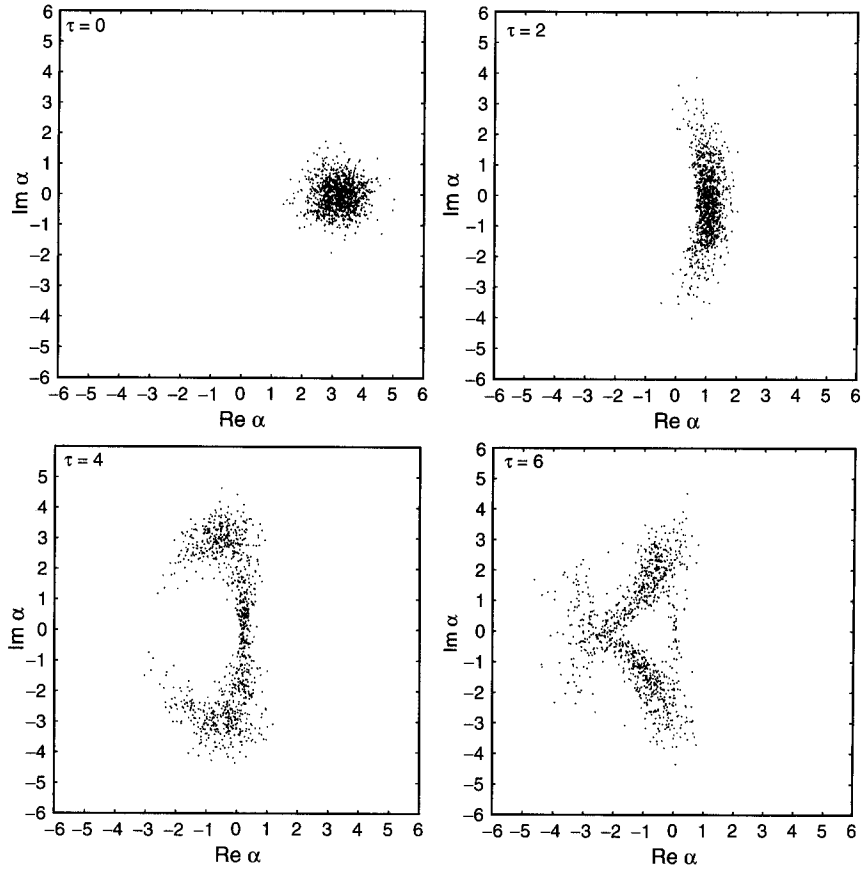

Figure 12. Classical trajectories for 1000 points for Gaussian distribution of initial values with unit variance and $N_a = 10$. Compare to Fig. 11a.

while the Q function does not suffer from such problems. When the initial state of the fundamental mode is a coherent state, the initial distribution is a Gaussian, and the result of simulation is pretty good. The method of classical trajectories has been used by Bajer et al. to explain the sub-Poissonian photon statistics in the second harmonic generation [36] as well as the third harmonic generation [37] in the no-energy-exchange regime. They have found that in this regime it is possible to obtain the steady-state solutions exhibiting sub-Poissonian photon statistics, and, surprisingly, they have shown that this quantum effect can be explained within the classical trajectories approach.

As we have already discussed in Section II, another characteristic of the quantum field is its phase distribution. The phase distribution of the quantum field can be calculated from the quasidistribution functions by integrating over the radial variable. In this way we get a kind of phase distribution that can be considered as an approximate description of the phase properties of the field. One can calculate the s-parametrized phase distributions, corresponding to the s-parametrized quasidistributions, for particular quantum states of the field [16]. However, a better way to study quantum phase properties is to use the Hermitian phase formalism introduced by Pegg and Barnett [11–13]. We have already introduced this formalism in Section II. Now, we apply this formalism to study the evolution of the phase properties of the two modes in the SHG process. In this case we have a two-mode field which requires a modification of the formulas presented in Section II into a two-mode case. The modification is rather trivial, and for the joint probability distribution for the continuous phase variables θ_a and θ_b describing phases of the two modes, we get the formula [53]

$$P(\theta_a, \theta_b) = \frac{1}{(2\pi)^2} \left| \sum_{n=0}^{\infty} b_n \sum_{k=0}^{[n/2]} c_{n,k}(t) \times \exp\{-i[(n-2k)\theta_a + k\theta_b - k(2\phi_a - \phi_b]\} \right|^2 \tag{143}$$

where ϕ_a and ϕ_b are the initial phases of the two modes, and the coefficients $c_{n,k}(t)$ are given by (122). The distribution (143) is normalized such that

$$\int_{-\pi}^{\pi} \int_{-\pi}^{\pi} P(\theta_a, \theta_b)\, d\theta_a\, d\theta_b = 1 \tag{144}$$

To choose the phase windows for θ_a and θ_b, we have to assign to ϕ_a and ϕ_b particular values. It is interesting to notice that formula (143) depends, in fact, on the difference $2\phi_a - \phi_b$, which reproduces the classical phase relation for the second harmonic generation, as seen in in classical equations (59). Classically, if there is no second-harmonic initially, this quantity must be $2\phi_a - \phi_b = \pm\pi/2$. This means that the phase of the second-harmonic mode is locked to the phase of the fundamental mode by this relation. It turns out that this is also a good choice to fix the phase windows in the quantum description. If the initial phase ϕ_a of the fundamental mode is zero, then $\phi_b = \pm\pi/2$ (depending on the sign of κ); that is, the second harmonic is shifted in phase by $\pi/2$ or $-\pi/2$ with respect to the fundamental mode.

The joint probability distribution given by Eq. (143) can be evaluated numerically and an example of such distribution is shown in Fig. 13, where the function $P(\theta_a, \theta_b)$ is plotted for several values of the scaled time τ and the initial mean number of photons of the fundamental mode $N_a = 10$. Initially the

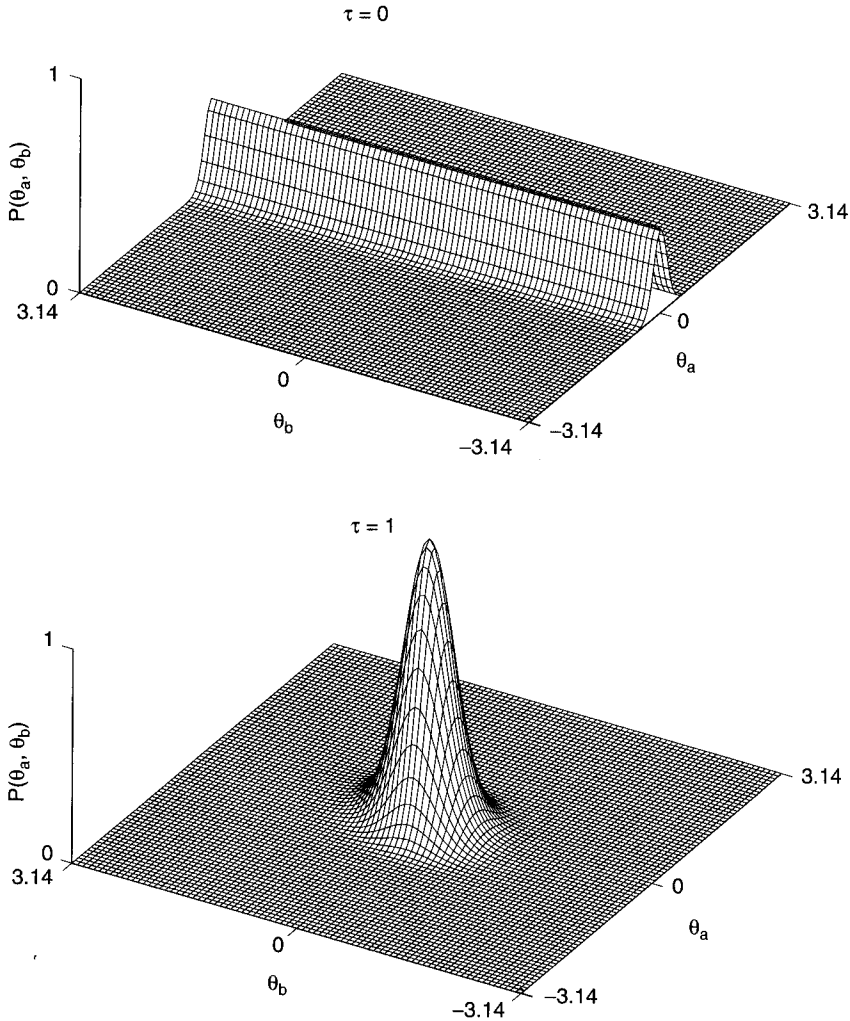

Figure 13. Joint phase probability distribution $P(\theta_a, \theta_b)$ of the fundamental and second-harmonic modes for various evolution time τ. In the last two figures the phase windows for θ_a and θ_b are shifted by π.

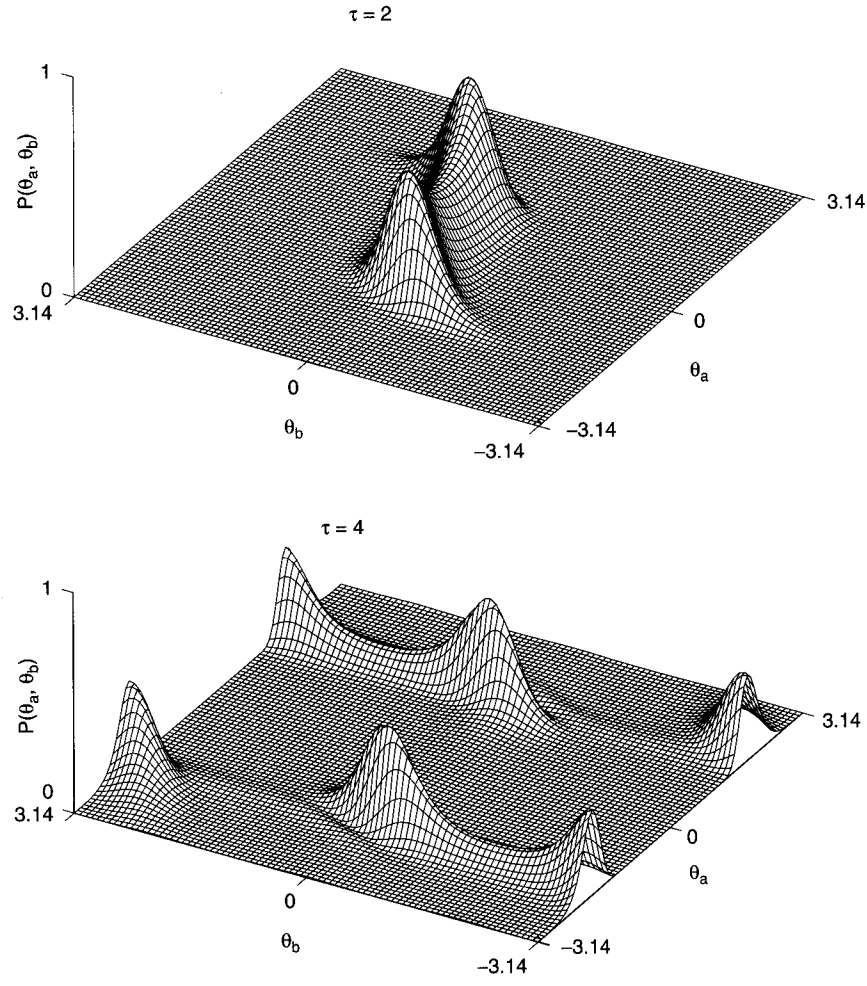

Figure 13. (*Continued*)

distribution is peaked at $\theta_a = 0$ in the θ_a direction reflecting the phase distribution of the coherent state of the fundamental mode, and it is completely flat in the θ_b direction reflecting the uniform phase distribution of the vacuum of the second-harmonic mode. At a later time, $\tau = 1$, a single, well-resolved peak of the distribution is visible, signifying a relatively well defined phase of the second-harmonic mode in conjunction with the phase of the fundamental mode. The fact that the peak appears for $\theta_a = \theta_b = 0$ corroborates the classical phase

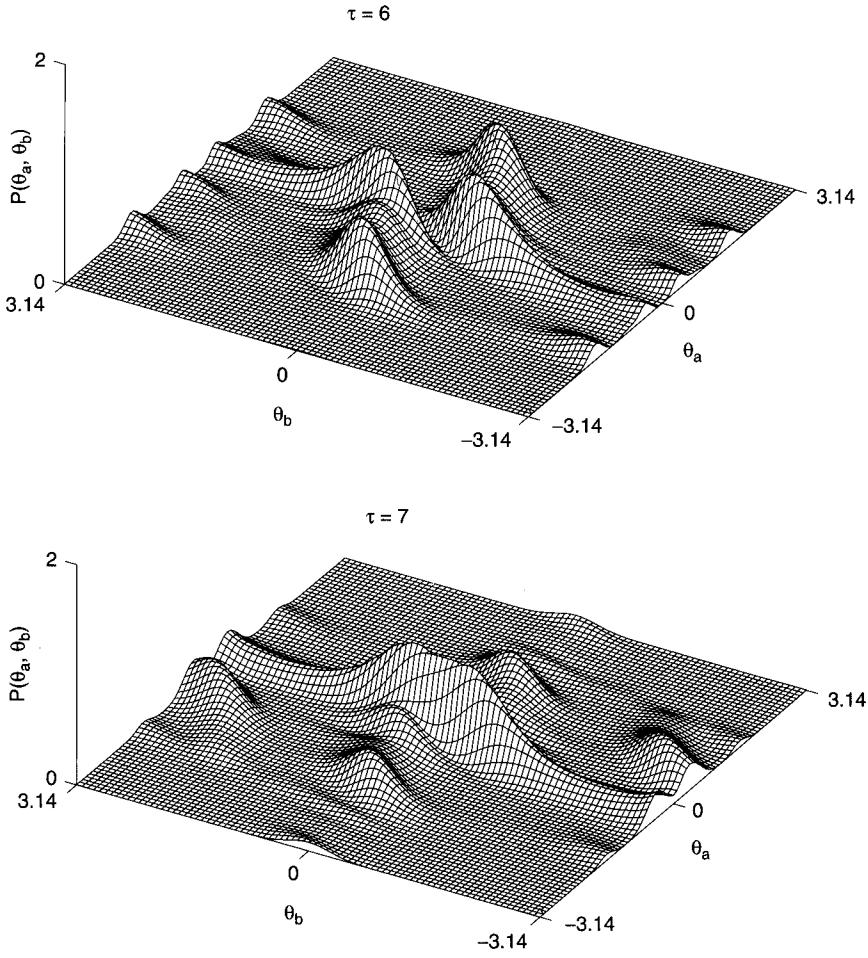

Figure 13. (*Continued*)

relation $2\phi_a - \phi_b = \pi/2$, which has been assumed here to choose the phase windows. As the evolution proceeds, for $\tau = 2$, the phase distribution $P(\theta_a, \theta_b)$ splits into two peaks. This is very interesting interval of time in which the second-harmonic mode achieves its maximum and the reverse process of downconversion start to predominate (can be seen from Fig. 5). The case of downconversion will be discussed later on, but now we can say that appearance of the two-peak phase distribution is a qualitative change in the phase properties

of the field, and it can be ascribed to the transition in the evolution from the harmonic generation regime into the downconversion regime. The two-peak structure of the ideal squeezed states has been indicated by Vaccaro and Pegg [54], and for the downconversion process with quantum pump by Gantsog et al. [55]. The splitting of the phase distribution into two peaks resembles the splitting of the Q function for the fundamental mode indicated by Nikitin and Masalov [24] which we have discussed earlier. The multipeak structure of the Q function or/and the phase distribution can be an indication that the field becomes a superposition of macroscopically distinguishable quantum states, the so-called Schrödinger cats [25,27,30,56]. For still longer times, $\tau = 4$, the intensity of the second-harmonic approaches its minimum and we observe a transition from the regime of downconversion back to the regime of second-harmonic generation, but this time with a quite different "initial" state. Such "bifurcations" of the phase distribution lead to a multipeak structure of the phase distribution, which means more and more uniform phase distribution. We would also draw attention to the jump in phase by π, which is clearly visible in the last two figures (compare to the classical phase evolution shown in Fig. 2). The fact that one peak splits into just two peaks is related to the fact that the process we discuss is the two-photon process. For example, for the three-photon downconversion the threefold symmetry of the distributions is observed [57]. Generally, the joint phase probability distribution carries quite a bit of useful information about the quantum state of the field. It is also important that for two-mode fields the joint phase probability distribution is a function of two variables θ_a and θ_b only, in contrast to the function $Q(\alpha, \beta)$, which is a function of four real variables Re α, Im α, Re β, Im β, so it is easy to visualize the two-mode field using the phase distribution while it is difficult to visualize the Q function in the phase space. Of course, the phase distribution obtained by integration of the quasidistributions is in this respect equally easy to handle as the Pegg–Barnett phase distribution even though the two functions are different. Generally, different distribution functions carry different information, but some properties of the field can be read out from all of them.

The phase distribution function (143) allows for calculations of the phase variances for the individual modes as well as the phase correlations between the two modes by performing simple integrations over the phase variables θ_a and θ_b. Detailed discussion of the phase properties of the fields can be found in Ref. 16, and we will not repeat it here. The material presented in this section has been chosen as to illustrate how quantum noise, which is an indispensable ingredient of quantum description of optical fields, can be incorporated into the theory of nonlinear optical phenomena, in particular the phenomenon of second-harmonic generation.

IV. DEGENERATE DOWNCONVERSION

A process on the one hand similar to the second-harmonic generation because it is described by the same Hamiltonian (54) but on the other hand opposite the second-harmonic generation because the initial conditions are interchanged, is the process of degenerate downconversion. For the second-harmonic generation initially there is no signal field at the second-harmonic frequency 2ω and there is a strong (coherent) field at the fundamental frequency ω. On the contrary, for the downconversion process initially there is no signal at frequency ω and there is a strong (coherent) field at the frequency 2ω, which is the pump mode in this process. As we have already discussed, we can talk about "pure" second-harmonic generation or downconversion only at the initial stage of the evolution with these particular initial conditions. At later times both processes compete with each other with domination of one of them between the subsequent maxima and minima of the signal intensity in a given mode. There is, however, one important difference between the two processes—the second-harmonic process can start even when the fields are classical, while the downconversion process must be triggered by quantum fluctuations.

The simplest and most often used approximation allowing for analytical solutions of the downconversion problem is the *parametric approximation*, in which it is assumed that the pump mode is a strong coherent field that remains undepleted during the evolution. The amplitude of this classical field is an external parameter on which the solutions for the signal field depend. Equations of motion for the downconversion process are the same as in (56)

$$\begin{aligned} \frac{d}{dt}\hat{a}(t) &= -2i\kappa\,\hat{a}^{+}(t)\hat{b}(t) \\ \frac{d}{dt}\hat{b}(t) &= -i\kappa\,\hat{a}^{2}(t) \end{aligned} \tag{145}$$

It is easy to note that for classical fields $\hat{a}(t) \to \alpha(t)$ and $\hat{b}(t) \to \beta(t)$, there is no nonzero solution for the signal field $\alpha(t)$ if $\alpha(0) = 0$. In the parametric approximation, the pump field at frequency 2ω is assumed to be constant classical field $\beta_0 = |\beta_0|\exp(i\phi_b)$. Within this approximation the first equation, Eq. 145, together with its Hermitian conjugate, can be solved analytically giving

$$\begin{aligned} \hat{a}(\tau) &= \hat{a}(0)\cosh\tau + \hat{a}^{+}(0)\sinh\tau\exp\left[i\left(\phi_b - \frac{\pi}{2}\right)\right] \\ \hat{a}^{+}(\tau) &= \hat{a}^{+}(0)\cosh\tau + \hat{a}(0)\sinh\tau\exp\left[-i\left(\phi_b - \frac{\pi}{2}\right)\right] \end{aligned} \tag{146}$$

where we have introduced the scaled time $\tau = 2|\beta_0|\kappa t$. The solutions (146) can be generated using the following squeezing operator

$$\hat{S}(\zeta) = \exp\left(\frac{1}{2}\zeta^* \hat{a}^2 - \frac{1}{2}\zeta \hat{a}^{+2}\right) \tag{147}$$

where the parameter $\zeta = i\tau$, in the following way [4]

$$\hat{a}(\tau) = \hat{S}^{-1}(\zeta)\hat{a}(0)\hat{S}(\zeta)\,, \qquad \hat{a}^+(\tau) = \hat{S}^{-1}(\zeta)\hat{a}^+(0)\hat{S}(\zeta) \tag{148}$$

Thus, the degenerate parametric oscillator, specifically, the downconversion process in the parametric approximation, performs the squeezing transformation, generating the *ideal squeezed states*, which have been widely discussed in the literature (see, e.g., Refs. 5 and 6 and papers cited therein). This material is well known, and we will not repeat it here. We rather concentrate on the cases when the parametric approximation is not applicable and the pump mode must be treated as a dynamical variable, the evolution of which must be taken into account. The quantum dynamics of the parametric oscillator has been studied by Kinsler and Drummond [58]. Reid and Krippner [59] have found that a macroscopic superposition states can be created in the nondegenerate parametric oscillator. Mode entanglement in such a system has been studied by Drobný et al. [60]. Here, we focus on comparison of the quantum properties of fields produced in the downconversion to those produced in the second-harmonic generation using the same theoretical methods.

A. Symbolic Calculations

Let us start with the short-time approximation in which we can use the symbolic manipulation computer program described in Appendix A to find the corrections coming from the quantum fluctuations of the fields. The operator formulas (94) and (95) are valid also for the degenerate downconversion because the two processes are governed by the same Hamiltonian, but now initially the second-harmonic mode is populated while the fundamental mode is initially in the vacuum state. Assuming that the pump mode at the frequency 2ω is in a coherent state $|\beta_0\rangle$ ($\beta_0 = \sqrt{N_b}\exp(i\phi_b)$), we have

$$\begin{aligned} \langle \hat{a}(t) \rangle &= 0 \\ \langle \hat{b}(t) \rangle &= \beta_0 \left[1 - (\kappa t)^2 - \frac{1}{6}(\kappa t)^4 (8|\beta_0|^2 - 1) + \cdots \right] \end{aligned} \tag{149}$$

It is interesting to note that the mean value of the signal mode at frequency ω is zero, and it is true for all powers in the expansion, reflecting the fact that photons are created in pairs. In case of pump mode, we see that the amplitude of the field will evolve in time and the lowest nonzero term is the quadratic term. The fact that the mean field of the signal mode is zero explains why the signal mode is said to be in the *squeezed vacuum*. Another interesting and characteristic feature of such field is the fact that the mean value of the square of the annihilation operator is nonzero

$$\begin{aligned}\langle \hat{a}^2(t)\rangle &= -2i\beta_0\left[(\kappa t)+\frac{1}{3}(\kappa t)^3(8|\beta_0|^2-1)+\cdots\right]\\ &= \exp[i(\phi_b-\pi/2)]\left[\tau+\frac{2}{3}\tau^3\left(1-\frac{1}{8N_b}\right)+\cdots\right]\end{aligned} \tag{150}$$

and this fact justifies the name the *two-photon coherent state* introduced by Yuen [61].

Let us take a look at the mean number of photons in the signal mode, which up to the fourth order is given by

$$\begin{aligned}\langle \hat{a}^+(t)\hat{a}(t)\rangle &= 4|\beta_0|^2\left[(\kappa t)^2+\frac{2}{3}(\kappa t)^4(2|\beta_0|^2-1)+\cdots\right],\\ &= \tau^2+\frac{\tau^4}{3}\left(1-\frac{1}{2N_b}\right)+\cdots\end{aligned} \tag{151}$$

where we have introduced the scaled time $\tau = 2\sqrt{N_b}\kappa t$, as suggested by the solutions (146) in the parametric approximation. The last term, $\sim N_b^{-1}$, comes from the field commutator and represents the quantum noise. The other terms are the terms of the expansion of $\sinh^2\tau$, which is the mean number of photons in the parametric approximation given by the solutions (146). For the pump mode we have

$$\begin{aligned}\langle \hat{b}^+(t)\hat{b}(t)\rangle &= |\beta_0|^2\left[1-2(\kappa t)^2-\frac{4}{3}(\kappa t)^4(2|\beta_0|^2-1)+\cdots\right]\\ &= N_b-\frac{1}{2}\tau^2-\frac{1}{6}\tau^4\left(1-\frac{1}{2N_b}\right)+\cdots\end{aligned} \tag{152}$$

Again, we can easily identify the noise term, and moreover, it is clear from Eqs. (151) and (152) that the quantity $\langle \hat{a}^+(t)\hat{a}(t)\rangle + 2\langle \hat{b}^+(t)\hat{b}(t)\rangle = 2|\beta_0|^2 = 2N_b$ is conserved including the quantum noise terms.

Similarly, we obtain corresponding expressions for the quadrature variances

$$\begin{aligned}\langle[\Delta\hat{Q}_a]^2\rangle &= 1+4(\kappa t)\,\mathrm{Im}\,\beta_0+8(\kappa t)^2|\beta_0|^2+\frac{4}{3}(\kappa t)^3\,\mathrm{Im}\,\beta_0(8|\beta_0|^2-1)\\ &\quad+\frac{16}{3}(\kappa t)^4|\beta_0|^2(2|\beta_0|^2-1)+\cdots\\ &= 1+2\tau\sin\phi_b+2\tau^2+\frac{4}{3}\tau^3\sin\phi_b\left(1-\frac{1}{8N_b}\right)\\ &\quad+\frac{2}{3}\tau^4\left(1-\frac{1}{2N_b}\right)+\cdots \qquad (153)\\ \langle[\Delta\hat{P}_a]^2\rangle &= 1-4(\kappa t)\,\mathrm{Im}\,\beta_0+8(\kappa t)^2|\beta_0|^2-\frac{4}{3}(\kappa t)^3\,\mathrm{Im}\,\beta_0(8|\beta_0|^2-1)\\ &\quad+\frac{16}{3}(\kappa t)^4|\beta_0|^2(2|\beta_0|^2-1)+\cdots\\ &= 1-2\tau\sin\phi_b+2\tau^2-\frac{4}{3}\tau^3\sin\phi_b\left(1-\frac{1}{8N_b}\right)\\ &\quad+\frac{2}{3}\tau^4\left(1-\frac{1}{2N_b}\right)+\cdots \qquad (154)\end{aligned}$$

The sign of the linear terms in (153) and (154) depends on the sign of $\mathrm{Im}\beta_0$, and this sign decides whether the quadrature is squeezed. These examples illustrate the effectiveness of the symbolic manipulation programs in obtaining such expansions. Previously such calculations have been performed by hand. This approach belongs to the standard methods of quantum optics, and many results based on the power series expansion have been discussed in the book [62], so we restrict ourselves to these few examples only.

B. Numerical Methods

The exact operator expansions presented in the previous section indicated that the parametric approximation fails for sufficiently long evolution times, and, moreover, the quantum character of the pump mode introduces corrections to the field evolution coming from the quantum noise. Since the two parts of the Hamiltonian $\hat{H}_0$ and $\hat{H}_I$ given by Eq. (55) are constants of motion, again we can split the Hilbert space into orthogonal sectors, as before, and introduce for a given number n of the pump mode at frequency 2ω the states

$$|\psi_k^{(n)}\rangle = |2k, n-k\rangle\,, \qquad k=0,1,\ldots,n \qquad (155)$$

which again form a complete orthogonal basis of states in a sector with given n. Now, however, n is the number of photons of the second-harmonic mode, which

would correspond energetically to the $2n$ photons of the fundamental mode, so the dimension of the sector with given n is $(n+1)\times(n+1)$. Assuming that the initial state of the pump mode is a coherent state $|\beta_0\rangle$ and the signal mode at frequency ω is in the vacuum, we can define the initial state of the field as

$$|\psi(0)\rangle = \sum_{n=0}^{\infty} b_n e^{in\phi_b}|0,n\rangle \tag{156}$$

where

$$b_n = \exp\left(\frac{-N_b}{2}\right)\frac{N_b^{n/2}}{\sqrt{n!}} \tag{157}$$

where $N_b = |\beta_0|^2$, and ϕ_b is the initial phase of the pump field $[\beta_0 = |\beta_0|\exp(i\phi_b)]$. With these initial conditions the resulting state of the field is given by

$$|\psi(t)\rangle = \sum_{n=0}^{\infty} b_n e^{in\phi_b}\sum_{k=0}^{n} c_{2n,k}(t)|2k, n-k\rangle \tag{158}$$

where the coefficients $c_{2n,k}(t)$ are the matrix elements of the evolution operator

$$\begin{aligned} c_{2n,k}(t) &= \left\langle 2k, n-k\left|\exp\left(\frac{-i\hat{H}_I t}{\hbar}\right)\right|0,n\right\rangle \\ &= \sum_{j=0}^{n} e^{-i\lambda_j \kappa t} U_{n-k,j} U_{n,j}^{*} \end{aligned} \tag{159}$$

Comparing Eqs. (122) and (159), it is clear that the coefficients $c_{n,k}(t)$ and $c_{2n,k}(t)$ are derived from the same matrix U diagonalizing the Hamiltonian $\hat{H}_I$, but they include different elements of the matrix. As before, the coefficients (159) can be calculated numerically by diagonalizing the interaction Hamiltonian $\hat{H}_I$ [55]. The mean number of photons in both modes can be expressed, using the state (158), in the form

$$\begin{aligned} \langle \hat{N}_a(t)\rangle &= \langle \psi(t)|\hat{a}^{+}\hat{a}|\psi(t)\rangle = \sum_{n=0}^{\infty} b_n^2 \sum_{k=0}^{n} 2k|c_{2n,k}(t)|^2 \\ \langle \hat{N}_b(t)\rangle &= \langle \psi(t)|\hat{b}^{+}\hat{b}|\psi(t)\rangle = \sum_{n=0}^{\infty} b_n^2 \sum_{k=0}^{n} (n-k)|c_{2n,k}(t)|^2 \end{aligned} \tag{160}$$

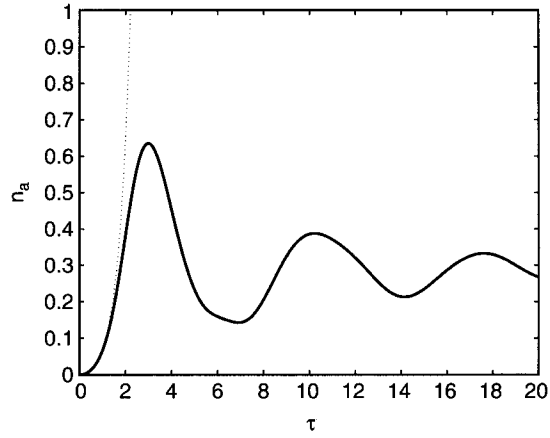

Figure 14. Signal intensity of the degenerate downconverter for the mean number of pump photons $N_b = 10$. Dotted line illustrates the parametric approximation.

where b_n is given by (157). In Fig. 14 we have plotted the signal intensity $n_a = \langle \hat{N}_a(\tau) \rangle / (2N_b)$ at frequency ω as a function of the scaled time $\tau = 2|\beta_0|\kappa t$. The intensity n_a is scaled in such a way that unity at the figure would mean the 100% conversion ratio. For reference we have plotted the normalized signal intensity in the parametric approximation, which is given by $\sinh^2 \tau/(2N_b)$. It is seen that the parametric approximation is valid for $\tau \leq 1$, and it fails for longer evolution times. As in the case of second-harmonic generation, the signal intensity exhibits damped oscillations; however, there is one important difference between the second-harmonic generation and the downconversion process, namely, the conversion ratio that can be achieved in both processes. As it is evident from Fig. 5b as the mean number of photons of the fundamental mode increases, the maximum conversion ratio also increases, becoming closer and closer to 100% efficiency. From Fig. 14 we see that the maximum conversion is below 70% for $N_b = 10$, and contrary to the second-harmonic generation, as the mean number of photons N_b of the pump mode increases the maximum conversion decreases. This effect is illustrated in Fig. 15, where we have plotted the maximum values of the scaled signal intensity n_a as a function of the mean number of photons of the pump mode N_b. This rather counterintuitive result has been discussed by Drobný and Bužek [63] who have found that there is a fundamental limit on the energy transfer in the k-photon downconversion. There is always a fraction of energy that is trapped in the pump mode and cannot be transferred to the downconversion signal and this fraction increases as the intensity of the pump mode becomes higher. If the dynamics of the pump mode

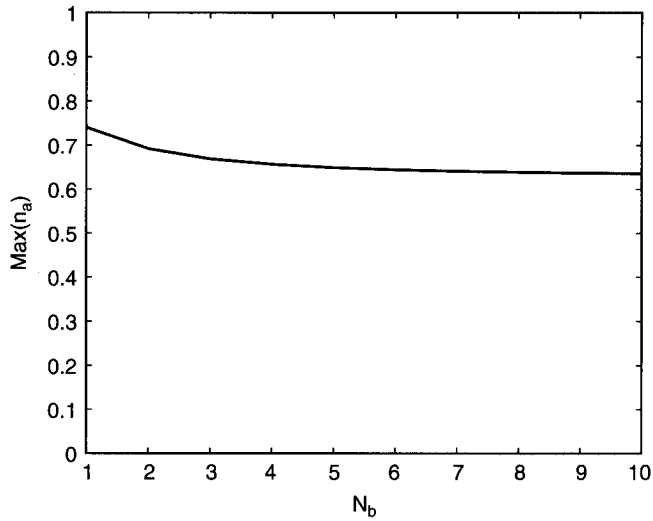

Figure 15. Maximum efficiency of energy transfer in the degenerate downconversion versus the initial mean photon number N_b of the pump mode.

is taken into account the downconversion signal behaves quite differently from the the idealized case when the parametric approximation is done.

The degenerate parametric downconversion is a source of squeezed light, which, as far as the parametric approximation is valid, produces the ideal squeezed states with the quadrature variances $\langle[\Delta\hat{Q}_a]^2\rangle = \exp(-2\tau)$ and $\langle[\Delta\hat{P}_a]^2\rangle = \exp(2\tau)$, which means that for $\tau \to \infty$, one of the variances goes to zero while the other goes to infinity. Thus, the idealized model allows for perfect squeezing. Of course, in a more realistic model in which the quantum noise of the pump mode is taken into account the amount of squeezing that can be obtained is limited. The two quadrature variances calculated numerically for $N_b = 10$ and $\phi_b = -\pi/2$ are illustrated in Fig. 16. For short evolution times τ the variance $\langle[\Delta\hat{Q}_a(\tau)]^2\rangle$ is squeezed, that is, it takes values below unity, that is below the vacuum fluctuations level. The $\hat{Q}$ quadrature is squeezed for the particular choice of the phase of the pump field, $\phi_b = -\pi/2$, in agreement with the analytical results presented in Eq. (99). For $\phi_b = 0$ both quadratures are unsqueezed. The dependence of squeezing on the field phase is a characteristic feature of this effect. The $\hat{Q}$ quadrature variance reaches a minimum below $\tau = 1$ and next shows maxima and minima that, however, do not fall below unity. It is a well-known fact that when the depletion of the pump mode and its quantum character is taken into account, the quadrature noise has finite minimum, and it has been shown [64–66] that the value of squeezing is

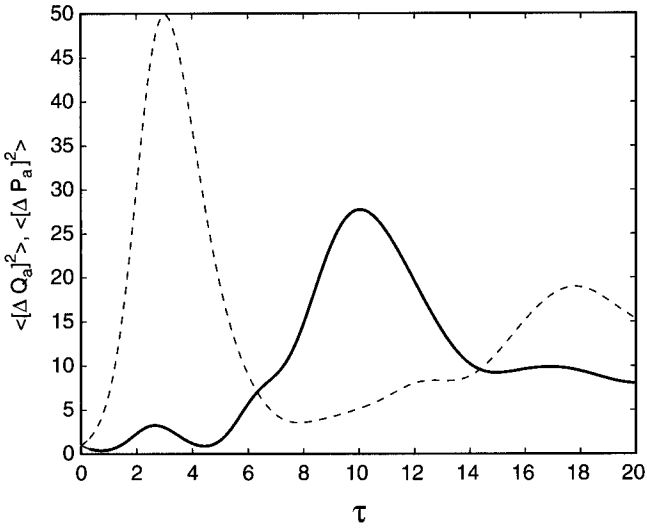

Figure 16. Quadrature variances of the signal mode for $N_b = 10$ and $\phi_b = -\pi/2$: $\langle[\Delta\hat{Q}_a(\tau)]^2\rangle$ (solid line) and $\langle[\Delta\hat{P}_a(\tau)]^2\rangle$ (dashed line).

bounded by $(2\sqrt{N_b})^{-1}$. Kinsler et al. [66] compared various numerical methods, including the number-state calculations and stochastic simulations based on the stochastic differential equations derived from the positive P representation. Here, we use the method of diagonalization of the Hamiltonian in the number-state basis, which is simple but it is applicable only for the pump fields with a not-too-large mean number of photons. Nevertheless, the results obtained in this simple way illustrate pretty well the features of the field produced in the degenerate down converter with quantum pump. In Fig. 17 we have plotted the quadrature variances for several values of the mean number of photons of the pump mode. It is seen that, as the number of photons increases, the solutions remain close to the parametric approximation for longer times, or in other words, the parametric approximation is valid longer as the pump fields are becoming stronger.

Similarly to the second-harmonic generation, we can calculate the Q function for the fields. With the state (158) we find for the two-mode field the formula

$$Q(\alpha,\beta) = \frac{1}{\pi^2}\mathrm{e}^{-(|\alpha|^2+|\beta|^2)}\left|\sum_{n=0}^{\infty} e^{in\phi_b} b_n \sum_{k=0}^{n} \frac{(\alpha^*)^{2k}(\beta^*)^{n-k}}{\sqrt{(2k)!(n-k)!}} c_{2n,k}(t)\right|^2 \qquad (161)$$

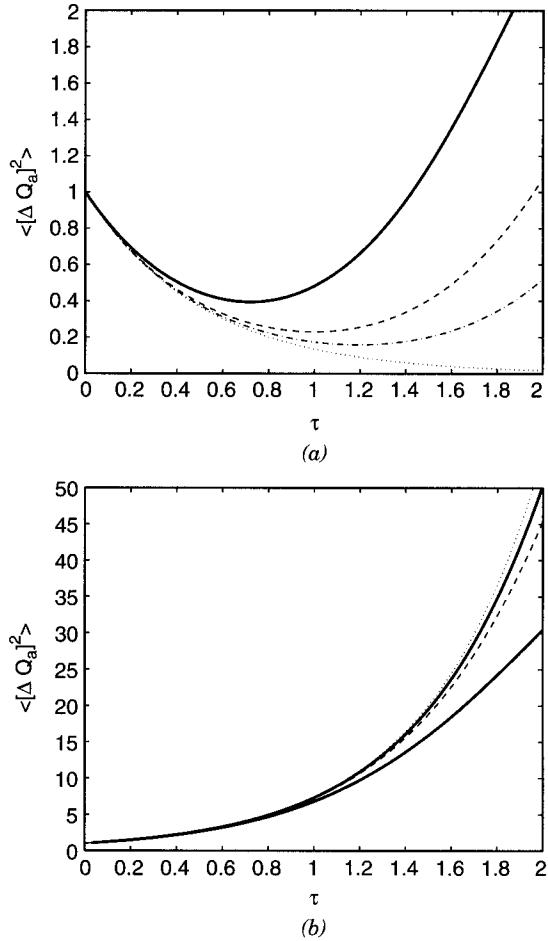

Figure 17. Quadrature variances (a) $\langle[\Delta\hat{Q}_a(\tau)]^2\rangle$ and (b) $\langle[\Delta\hat{P}_a(\tau)]^2\rangle$ for the signal mode with $\phi_b = -\pi/2$ and $N_b = 10$ (solid line), $N_b = 40$ (dashed line), and $N_b = 100$ (dashed–dotted line). Dotted lines represent parametric approximation.

which after corresponding integrations gives the Q functions for individual modes. For the signal mode, we have

$$Q(\alpha) = \frac{1}{\pi} e^{-|\alpha|^2} \sum_{n=0}^{\infty}\sum_{n'=0}^{\infty} e^{i(n-n')\phi_b} b_n b_{n'} \times \sum_{k=0}^{n}\sum_{k'=0}^{n'} \frac{(\alpha^*)^{2k}\alpha^{2k'}}{\sqrt{(2k)!(2k')!}} c_{2n,k}(t) c^*_{2n',k'}(t)\delta_{n-k,n'-k'} \tag{162}$$

and for the pump mode

$$Q(\beta) = \frac{1}{\pi} e^{-|\beta|^2} \sum_{n=0}^{\infty} \sum_{n'=0}^{\infty} e^{i(n-n')\phi_b} b_n b_{n'} \times \sum_{k=0}^{\min(n,n')} \frac{(\beta^*)^{n-k} \beta^{n'-k}}{\sqrt{(n-k)!(n'-k)!}} c_{2n,k}(t) c^*_{2n',k}(t) \tag{163}$$

where the coefficients $c_{2n,k}(t)$ are given by (159) and the Poissonian factors b_n, by (157). The contours of the Q functions for the signal (Fig. 18a) and pump (Fig. 18b) modes, for a particular choice of the evolution times, are illustrated in Fig. 18. The squeezing property of the signal is clearly seen for $\tau = 1$, and for a longer time $\tau = 3$ the Q function of the signal mode develops a two-peak structure. All the time the mean amplitude of the signal mode is zero — the quasidistribution exhibits a twofold symmetry around the origin. The pump mode starts from a coherent state with the amplitude $-i\sqrt{10}$, and next the distribution is smeared along the imaginary axis ($\tau = 3$) and concentrates again to an approximately coherent state with the amplitude $i\sqrt{10}$ ($\tau = 6$). It is interesting to compare the shape of the Q functions with the maxima and minima of the intensity of the signal mode shown in Fig. 14.

The classical trajectories approach, described in Section III.D, applied to the downconversion regime confirms pretty well the fully quantum calculations for the quasidistribution functions presented in Fig. 18. Examples of the classical trajectories approach are shown in Fig. 19. Similarly to the second-harmonic generation (see Section III.D), the initial values are taken from the Gaussian distribution with the appropriately adjusted variance and the set of classical equations (59) is solved numerically for 1000 trajectories. As it is evident from Fig. 19, the cloud of points reproduces very well the quasidistribution functions for both modes. The classical trajectories approach has an advantage over the direct quantum calculations with the diagonalization of the Hamiltonian in this that it can be applied to the fields with large number of photons where the diagonalization method cannot be used because of the computer limitations. It has been shown [52] that the Wigner function is the most adequate quasidistribution function to use with classical trajectories approach, and the symmetric ordering associated with the Wigner function should be used to calculate mean values of the physical quantities by averaging over ensembles of classical trajectories. Here we have illustrated both approaches, choosing the mean number of photons $N_b = 10$ for which the calculations can be performed even on small computers.

The Hermitian operator phase formalism of Pegg and Barnett [11–13] allows for quantum calculations of phase distribution for the fields produced in the

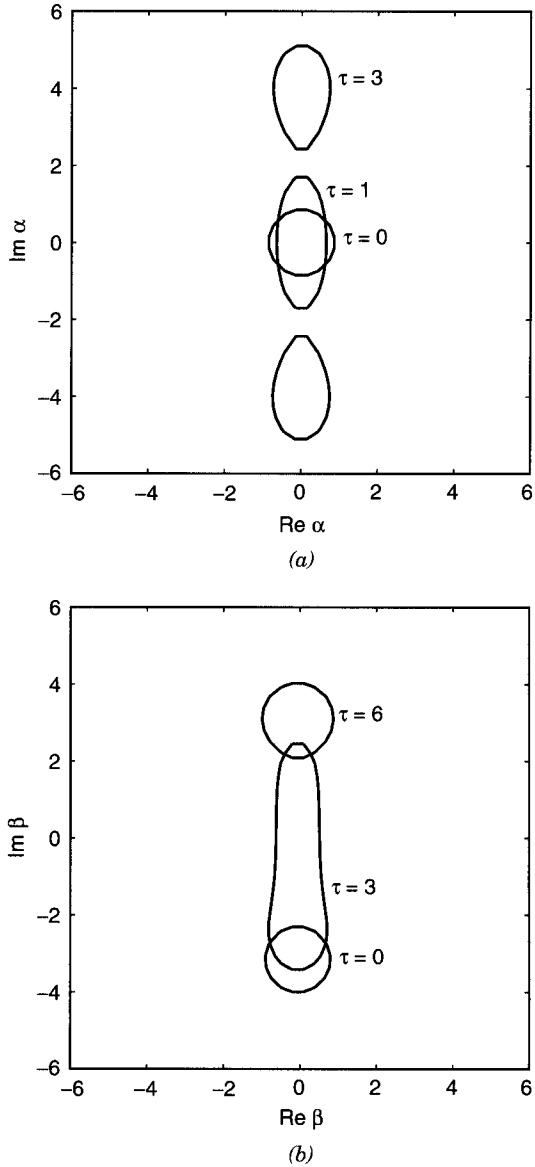

Figure 18. Contour plots of the Q function for (a) the signal mode and (b) pump mode for $N_b = 10, \phi_b = -\pi/2$, and several values of the evolution time τ. Contours are taken at half the maximum.

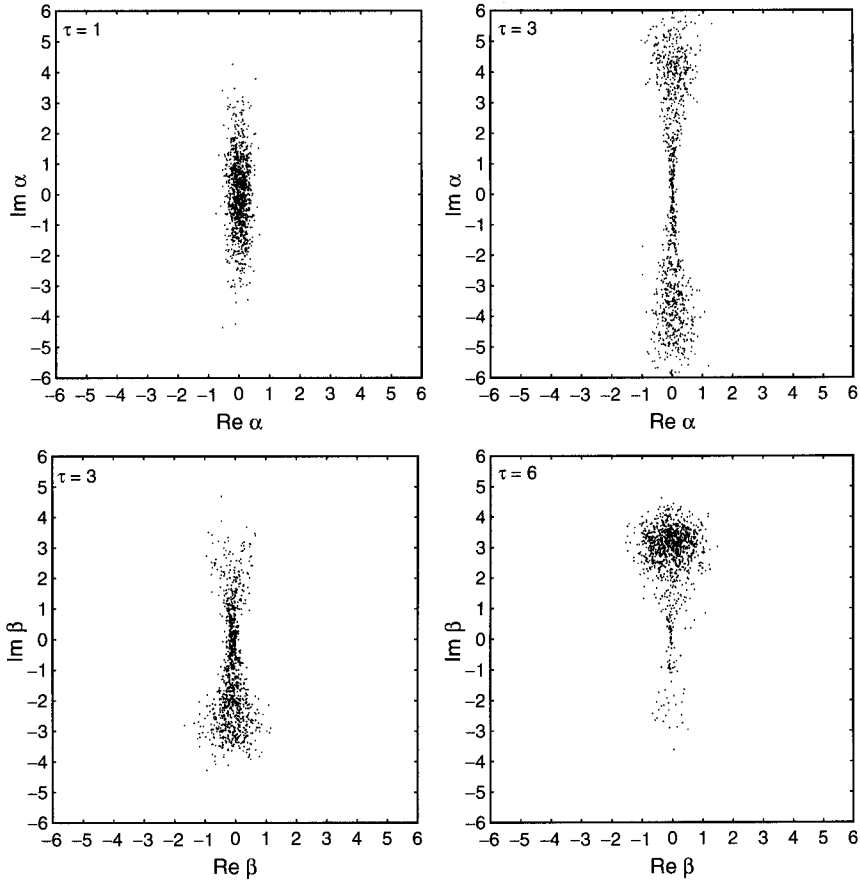

Figure 19. Classical trajectories for 1000 points for Gaussian distribution of initial values and $N_b = 10, \phi_b = -\pi/2$ for the signal mode (upper figures) and the pump mode (lower figures). The evolution times are chosen as to compare with Fig. 18.

downconversion process [55]. The joint phase probability distribution has the following form in this case [16,55]:

$$P(\theta_a, \theta_b) = \frac{1}{(2\pi)^2} \left| \sum_{n=0}^{\infty} b_n \sum_{k=0}^{n} c_{2n,k}(t) \right.$$
$$\left. \times \exp\{-i[2k\theta_a + (n-k)\theta_b + k(2\phi_a - \phi_b)]\} \right| \qquad (164)$$

It is very instructive to compare the joint phase probability distributions for the signal and pump modes produced in the downconversion process shown in

Fig. 20 to the same distribution for the fields produced in the second-harmonic generation process shown in Fig. 13. The differences are clearly visible. The distribution for the downconverted field from the beginning develops a two-peak phase structure, which is a consequence of the two-fold rotational symmetry of the Q function for the signal mode. It is known [57,67] that for k-photon downconversion the Q function has k-fold rotational symmetry and the phase distribution has k peaks, at least at the initial stages of the evolution. From Fig. 20 it is also clear that when the intensity of the signal mode reaches its

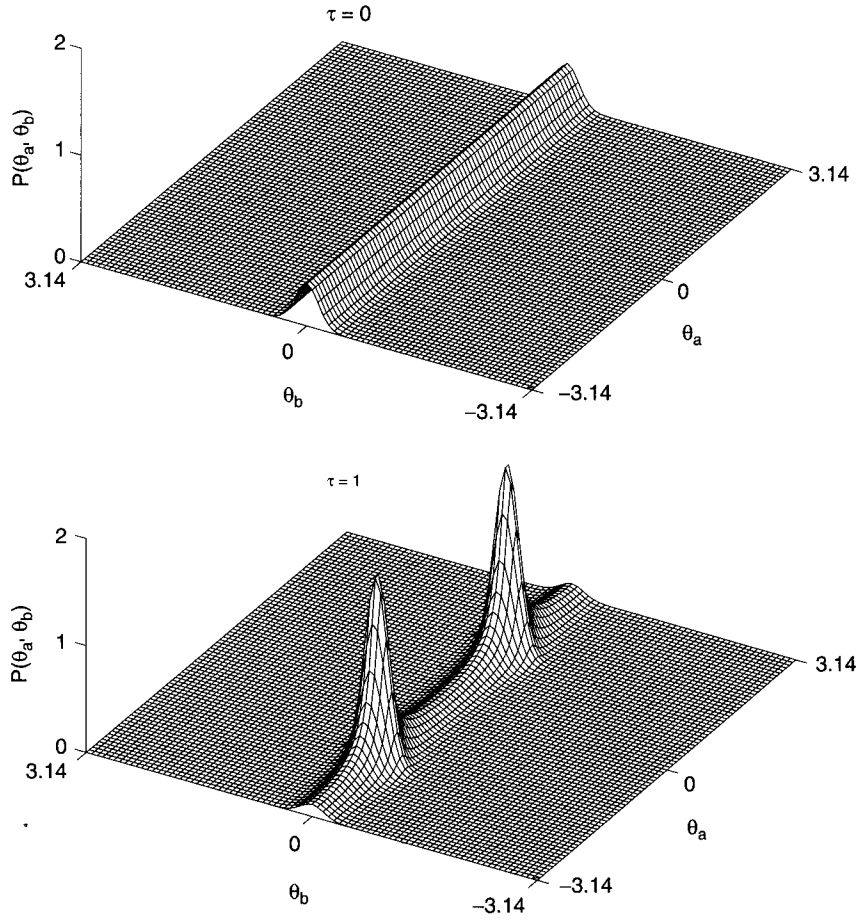

Figure 20. Joint phase probability distribution $P(\theta_a, \theta_b)$ for the signal and pump modes at several evolution times τ and $N_b = 10$. In the last two figures the window for θ_b is shifted $\theta_b \to \theta_b + \pi/2$ and $\theta_b \to \theta_b + \pi$, correspondingly.

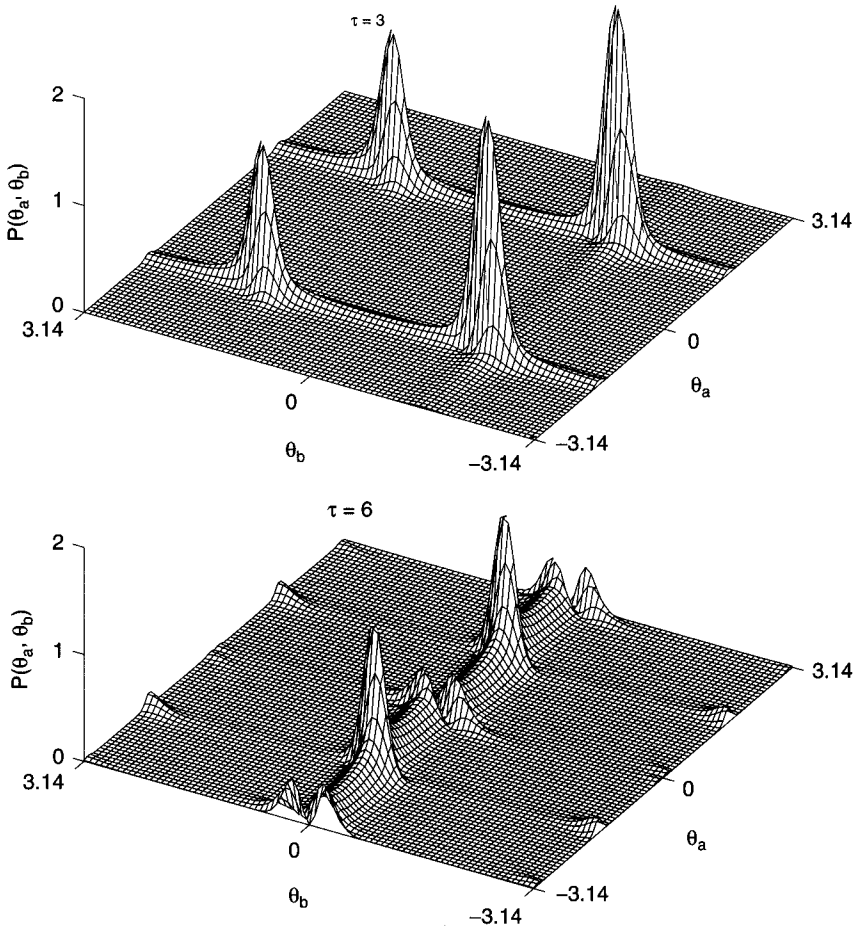

Figure 20. (*Continued*)

maximum ($\tau = 3$), the process is reversed from the downconversion regime to the harmonics generation regime and the phase distribution for θ_b splits into two peaks and a jump in phase by $\pi/2$ appears. For $\tau = 6$, the phase distribution confirms the fact seen from the contours of the Q function, that the pump mode reaches the state close to the initial coherent state but shifted in phase by π. To avoid splitting of the peaks in the phase distribution, we have made corresponding shifts of the phase window for θ_b variable for the last two pictures of Fig. 20, so $\theta_b \to \theta_b + \pi/2$ and $\theta_b \to \theta_b + \pi$, correspondingly. The two-peak structure of the phase distribution is a characteristic feature of the ideal squeezed states. To

compare the ideal squeezed state phase distribution with the distribution for downconversion with quantum pump, we can calculate the marginal phase distribution functions, which are obtained by integrating (164) over one of the phase variables. The result is

$$P(\theta_a) = \frac{1}{2\pi}\left\{1 + 2\mathrm{Re}\sum_{n>n'} b_n b_{n'} \sum_{k=0}^{n}\sum_{k'=0}^{n'} c_{2n,k}(t)c^*_{2n',k'}(t) \times \exp[-i(k-k')(2\theta_a + 2\phi_a - \phi_b)]\delta_{n-n',k-k'}\right\}$$

$$P(\theta_b) = \frac{1}{2\pi}\left\{1 + 2\mathrm{Re}\sum_{n>n'} b_n b_{n'} \sum_{k=0}^{n'} c_{2n,k}(t)c^*_{2n',k}(t) \times \exp[-i(n-n')\theta_b]\right\} \tag{165}$$

The marginal phase distributions are illustrated in Fig. 21a, where we have plotted the phase distribution $P(\theta_a)$ for the signal mode at the evolution time $\tau = 1$ and the phase distribution for the ideal squeezed state for the same squeezing parameter. The mean number of photons for the pump mode is equal to 10. It is clear that quantum fluctuations of the pump mode cause broadening of the phase distribution, but the two-peak structure of the distribution with the peaks at $\pm\pi/2$ is obvious. For large squeezing, the phase distribution of the ideal squeezed state becomes the sum of two symmetrically placed delta functions

$$P(\theta_a) = \frac{1}{2}\left[\delta\left(\theta_a - \frac{\pi}{2}\right) + \delta\left(\theta_a + \frac{\pi}{2}\right)\right] \tag{166}$$

but the quantum noise present in the pump mode broadens the phase distribution which can never become the delta function distribution. In Fig. 21b we have shown the distribution for the pump mode at the evolution time $\tau = 6$, which is compared to the initial coherent state phase distribution (dotted line). The window for θ_b is shifted by π to be consistent with Fig. 20. The phase distribution of the pump mode for this particular evolution time corroborates what has already been found from previous figures, that at time $\tau = 6$ the state of the pump mode becomes close to the coherent state but shifted in phase by π with respect to the initial state. This illustrates that the phase distribution is a very convenient function to study in order to get information about the quantum state of the field.

Because of the oscillatory behavior of the intensity of the signal mode, which switches the process from the downconversion regime to the second-harmonic

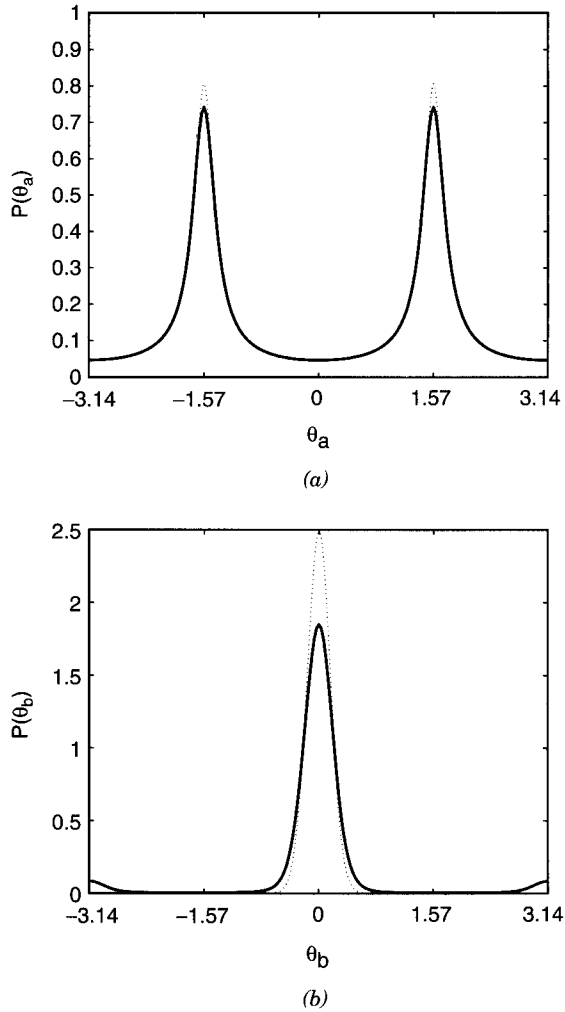

Figure 21. Marginal phase distributions: (a) $P(\theta_a)$ for $\tau = 1$ (solid line) and ideal squeezed vacuum (dotted line); (b) $P(\theta_b)$ for $\tau = 6$ (solid line) and coherent state with $N_b + 10$ (dotted line). The window for θ_b is shifted by π.

generation regime and back, the structure of the joint phase distribution $P(\theta_a, \theta_b)$ for longer evolution times becomes more complicated. This is true for both the phase distribution that started in the pure SHG regime and the distribution that started in the pure downconversion regime. As the evolution proceeds the subsequent bifurcations of the distribution take place and the effect

of quantum noise accumulates, making the phase distributions more and more flat indicating randomization of the phase. More details on the quantum phase properties of the fields produced in nonlinear optical phenomena can be found in Ref. 16.

V. SUMMARY

In this chapter we have discussed two best-known nonlinear optical phenomena — second-harmonic generation and parametric downconversion — drawing particular attention to the signatures of quantum fluctuations of the optical fields that can be found in the phenomena. The ubiquitous vacuum fluctuations can manifest themselves in various ways when an optical field undergoes nonlinear transformation. The two processes considered here are only examples of a rich variety of nonlinear phenomena, but they are of great practical importance and thus they have been studied for years and a lot of knowledge has been accumulated. It was not our intention to collect all the facts known about the two processes, but rather to select some specific effects illustrating the role of quantum character of the field in the process. We have also presented several theoretical methods that are used to describe quantum properties of the field and are now available to everybody owing to common access to computers and software. Quantum fields are operator quantities that cannot be treated on computers in the same way as ordinary numbers describing classical quantities. However, presently existing computer software allows for symbolic manipulation, which makes it trivial to obtain formulas that would be very difficult or even impossible to obtain by hand. The early results indicating possibility of nonclassical effects such as sub-Poissonian photon statistics or squeezing were based on the power expansions of operator products. We have shown here how it can be done with freely available software using a computer. Also traditional numerical calculations became easy with the use of now existing numerical packages. We have presented examples of such calculations. We have compared quantum statistical properties of the fields produced in the idealized models of second-harmonic generation and downconversion with quantum pump using the same methods of symbolic calculations, approximate analytical methods, the method of classical trajectories with stochastic initial conditions and direct, fully quantum-mechanical calculations using the method of diagonalization of the interaction Hamiltonian. Since both processes discussed in this chapter are described by the same Hamiltonian, the differences between the quantum properties of the field generated in them have their origin in the initial conditions, in particular, in the presence of quantum fluctuations. As we have shown, the differences are quite important and their comparison is very instructive.

APPENDIX A

An example of the FORM [47] program calculating symbolically evolution of the operator $\hat{a}^+(t)\hat{a}(t)$ in the SHG process and the results produced by the program. The program calculates the Taylor series expansion terms up to given order (16 in the example). `T'n'` is the nth order term which must be multiplied by $(\kappa t)^n$, and the notation `ad(n)` means $(\hat{a}^+)^n$, and correspondingly `a(n)` means $\hat{a}^n$, where $\hat{a}$ and $\hat{a}^+$ are the annihilation and creation operators for the fundamental beam. In the calculations we assume that initially there are no photons of the second-harmonic beam, that is, after operator calculations we take the expectation value over the vacuum state for the second-harmonic beam. In the program this is performed by identifying $\hat{b}$ and $\hat{b}^+$ as zero after the normal ordering of the operators. The program is very simple (just few lines of code) and very effective (just few seconds on a Dual PIII 450 MHz machine under Linux).

```
FORM by J.Vermaseren. Version 1.1 Dec 14 1998

* calculates Taylor series terms for harmonics generation

  nwrite statistics;
  Symbols n,k;
  Function T,a,ad,b,bd,x,y;
  Set aa:a,ad;
  Set bb:b,bd;

* definitions

  #define MAX "16"
  * Hamiltonian
  Local H=ad*ad*b+a*a*bd;
  * operator the evolution we are looking for
  Local T0=ad*a;
  .sort

* main loop

  #do i=1,'MAX'
  Local T{'i'} = (T{'i'-1}*H-H*T{'i'-1})/i_/'i';
  repeat;
  id x?bb*y?aa=y*x;
  endrepeat;
  .sort
```

```
 repeat;
 id a*ad=ad*a+1;
 id b*bd=bd*b+1;
 endrepeat;
 .sort
 #enddo;
 id b=0;
 id bd=0;
 id x?=x(1);
 repeat;
 id x?(n?)*x?(k?)=x(n+k);
 endrepeat;
 print;
 .end

* results

 T0 = ad(1)*a(1);

 T1 = 0;

 T2 = - 2*ad(2)*a(2);

 T3 = 0;

 T4 = 8/3*ad(3)*a(3) + 4/3*ad(2)*a(2);

 T5 = 0;

 T6 = - 136/45*ad(4)*a(4) - 128/45*ad(3)*a(3) - 16/45*ad(2)*a(2);

 T7 = 0;

 T8 = 992/315*ad(5)*a(5) + 184/35*ad(4)*a(4) + 416/315*ad(3)*a(3)
    + 16/315*ad(2)*a(2);

 T9 = 0;

 T10 = - 44224/14175*ad(6)*a(6) - 4544/567*ad(5)*a(5) - 12128/
   2835*ad(4)*a(4)
     - 1024/2835*ad(3)*a(3) - 64/14175*ad(2)*a(2);

 T11 = 0;
```

```
T12 = 1398016/467775*ad(7)*a(7) + 730976/66825*ad(6)*a(6)
    + 914944/93555*ad(5)*a(5) + 67904/31185*ad(4)*a(4)
    + 2816/42525*ad(3)*a(3) + 128/467775*ad(2)*a(2);

T13 = 0;

T14 = - 118984832/42567525*ad(8)*a(8) - 65317888/4729725*
 ad(7)*a(7)
    - 12242816/654885*ad(6)*a(6) - 1856000/243243*ad(5)*a(5)
    - 4741376/6081075*ad(4)*a(4) - 4096/467775*ad(3)*a(3)
    - 512/42567525*ad(2)*a(2);

T15 = 0;

T16 = 1639572992/638512875*ad(9)*a(9) + 2102147456/
127702575*ad(8)*a(8)
    + 20049444736/638512875*ad(7)*a(7) + 378236224/
   18243225*ad(6)*a(6)
    + 43331584/10135125*ad(5)*a(5) + 6365056/30405375*ad(4)*a(4)
    + 559616/638512875*ad(3)*a(3) + 256/638512875*ad(2)*a(2);
```

APPENDIX B

An example of the program that can be run using the free available software OCTAVE [50] (under Linux) or the commercial software MATLAB [51] (under Linux or MS Windows). The program calculates numerically the intensity of the second-harmonic using the procedure of diagonalizing the interaction Hamiltonian described in the text (Section III.D).

```
% program intensity.m
% calculates the intensity of the second-harmonic
% using diagonalization of the interaction Hamiltonian
% int2 - second-harmonic intensity
% int1 - fundamental mode intensity

clear
nav=input(' mean number of photons: ');
nmax=input(' nmax: ');
tmax=input(' taumax: ');
t=0:tmax/511:tmax;

tic;
int2=zeros(1,512);
```

```
% Poisson distribution
b(1)=exp(-nav);
b(2)=b(1)*nav;
for n=2:nmax
b(n+1)=b(n)*nav/n;

% calculates the Hamiltonian H
nd=floor(n/2)+1;
nd1=floor((nd-1)/2);
hk=zeros(nd-1,1);
 for k=0:nd-2
 hk(k+1,1)=sqrt((k+1)*(n-2*k)*(n-2*k-1));
 end
 H=diag(hk,1)+diag(hk,-1);

% diagonalization with scaling
 [u e]=eig(H./sqrt(2*nav));
% [u e]=eig(H);
 [e l]=sort(diag(e));
 u=u(:,l);

% calculation of the intensity
 cz=0;
  for k=0:nd-1;
  c=0;
   if rem(k,2)==0;
    for l=0:nd1;
    c=c+u(k+1,l+1)*u(1,l+1)*cos(e(l+1,1)*t);
    end
   else
    for l=0:nd1;
    c=c+u(k+1,l+1)*u(1,l+1)*sin(e(l+1,1)*t);
    end
   end
  c=2*c;
    if rem(nd+1,2)==0;
    c=c-u(k+1,nd1+1)*u(1,nd1+1);
    end
  cz=cz+k*c.^2;
 end
 int2=int2+b(n+1)*cz;     % second-harmonic intensity
end
```

```
int1=nav-2*int2;        % fundamental intensity
r=int1/nav;
toc
plot(t,r);
xlabel('time'),ylabel('intensity ');
```

References

1. Y. R. Shen, *The Principles of Nonlinear Optics*, Wiley, New York, 1985.
2. S. Kielich, *Nonlinear Molecular Optics*, Nauka, Moscow, 1981 (in Russian).
3. C. W. Gardiner, *Quantum Noise*, Springer, Berlin, 1991.
4. P. L. Knight and R. Loudon, *J. Mod. Opt.* **34**, 709 (1987).
5. R. Loudon and P. L. Knight, *J. Mod. Opt.* **34**, 709 (1987).
6. M. C. Teich and B. E. A. Saleh, *Quantum Opt.* **1**, 153 (1989).
7. J. Peřina, *Quantum Statistics of Linear and Nonlinear Optical Phenomena*, 2 ed., Kluwer, Dordrecht, 1991.
8. L. Davidovich, *Rev. Mod. Phy.* **68**, 127 (1996).
9. L. Mandel, *Opt. Commun.* **42**, 437 (1982).
10. K. E. Cahill and R. J. Glauber, *Phys. Rev.* **177**, 1857 (1969).
11. D. T. Pegg and S. M. Barnett, *Europhys. Lett.* **6**, 483 (1988).
12. S. M. Barnett and D. T. Pegg, *J. Mod. Opt.* **36**, 7 (1989).
13. D. T. Pegg and S. M. Barnett, *Phys. Rev. A* **39**, 1665 (1989).
14. W. H. Louisell, *Quantum Statistical Properties of Radiation*, J Wiley, New York, 1973.
15. D. T. Pegg and S. M. Barnett, *Phys. Rev. A* **43**, 2579 (1991).
16. R. Tanaś, A. Miranowicz, and T. Gantsog, in E. Wolf (Ed.), *Progress in Optics*, Elsevier Scientific, Amsterdam, 1996, Vol. XXXV, pp. 355–446.
17. V. Peřinová, A. Lukš, and J. Peřina, *Phase in Optics*, World Scientific, Singapore, 1998.
18. P. A. Franken, A. E. Hill, C. W. Peters, and G. Weinreich, *Phys. Rev. Lett.* **7**, 118 (1961).
19. D. F. Walls and C. T. Tindle, *Nuovo Cimento Lett.* **2**, 915 (1971).
20. D. F. Walls and C. T. Tindle, *J. Phys. A* **5**, 534 (1972).
21. M. Kozierowski and R. Tanaś, *Opt. Commun.* **21**, 229 (1977).
22. L. A. Wu, H. J. Kimble, J. L. Hall, and H. Wu, *Phys. Rev. Lett.* **57**, 2520 (1986).
23. S. Kielich, M. Kozierowski, and R. Tanaś, *Optica Acta* **32**, 1023 (1985).
24. S. P. Nikitin and A. V. Masalov, *Quantum Opt.* **3**, 105 (1991).
25. B. Yurke and D. Stoler, *Phys. Rev. Lett.* **57**, 13 (1986).
26. P. Tombesi and A. Mecozzi, *J. Opt. Soc. Am. B* **4**, 1700 (1987).
27. A. Miranowicz, R. Tanaś, and S. Kielich, *Quantum Opt.* **2**, 253 (1990).
28. T. Gantsog and R. Tanaś, *J. Mod. Opt.* **38**, 1021 (1991).
29. G. S. Agarwal and R. R. Puri, *Phys. Rev. A* **40**, 5179 (1989).
30. T. Gantsog and R. Tanaś, *Quantum Opt.* **3**, 33 (1991).
31. J. Bajer and P. Lisoněk, *J. Mod. Opt.* **38**, 719 (1991).
32. J. Bajer and J. Peřina, *Opt. Commun.* **92**, 99 (1992).

33. R. F. Alvarez-Estrada, A. Gómez-Nicola, L. L. Sánchez-Soto, and A. Luis, *J. Phys. A* **28**, 3439 (1995).
34. T. Gantsog, R. Tanaś, and R. Zawodny, *Phys. Lett. A* **155**, 1 (1991).
35. G. Drobný and I. Jex, *Phys. Lett. A* **169**, 273 (1992).
36. J. Bajer, O. Haderka, and J. Peřina, *J. Opt. B: Quantum Semiclass. Opt.* **1**, 529 (1999).
37. J. Bajer, J. Peřina, O. Haderka, and A. Miranowicz, *Czech. J. Phys.* **50**, 717 (2000).
38. M. K. Olsen, R. J. Horowicz, L. I. Plimak, N. Treps, and C. Fabre, *Phys. Rev. A* **61**, 021803 (2000).
39. P. D. Drummond, K. J. McNeil, and D. F. Walls, *Optica Acta* **27**, 321 (1980).
40. P. D. Drummond, K. J. McNeil, and D. F. Walls, *Optica Acta* **28**, 211 (1981).
41. P. Szlachetka and K. Grygiel, "Chaos in optical systems", this volume.
42. A. Bandilla, G. Drobný, and I. Jex, *Opt. Commun.* **128**, 353 (1996).
43. G. Drobný, A. Bandilla, and I. Jex, *Phys. Rev. A* **55**, 78 (1997).
44. Z. Y. Ou, *Phys. Rev. A* **49**, 2106 (1994).
45. R. D. Li and P. Kumar, *Phys. Rev. A* **49**, 2157 (1994).
46. R. Tanaś, *Optik* **40**, 109 (1974).
47. J. A. M. Vermaseren, *FORM*, 1989, version 1 of the program is available from ftp.nikhef.nl.
48. J. Mostowski and K. Rzążewski, *Phys. Lett. A* **66**, 275 (1978).
49. D. F. Walls and R. Barakat, *Phys. Rev. A* **1**, 446 (1970).
50. J. W. Eaton, *GNU Octave. A High-Level Interactive Language for Numerical Computations*, (1997), OCTAVE is available from http://www.octave.org/,.
51. Matlab, is a product of The MathWorks, Inc., see http://www.mathworks.com.
52. D. Kupiszewska and K. Rzążewski, *Phys. Rev. A* **42**, 6869 (1990).
53. R. Tanaś, T. Gantsog, and R. Zawodny, *Quantum Opt.* **3**, 221 (1991).
54. J. A. Vaccaro and D. T. Pegg, *Opt. Commun.* **70**, 529 (1989).
55. T. Gantsog, R. Tanaś, and R. Zawodny, *Opt. Commun.* **82**, 345 (1991).
56. T. Gantsog and R. Tanaś, *J. Mod. Opt.* **38**, 1537 (1991).
57. R. Tanaś and T. Gantsog, *Phys. Rev. A* **45**, 5031 (1992).
58. P. Kinsler and P. D. Drummond, *Phys. Rev. A* **43**, 6194 (1991).
59. M. D. Reid and L. Křippner, *Phys. Rev. A* **47**, 552 (1993).
60. G. Drobný, I. Jex, and V. Buzek, *Phys. Rev. A* **48**, 569 (1993).
61. H. P. Yuen, *Phys. Rev. A* **13**, 2226 (1976).
62. J. Peřina, *Quantum Statistics of Linear and Nonlinear Optical Phenomena*, 2nd ed., Kluwer, Dordrecht, 1991.
63. G. Drobný and V. Bužek, *Phys. Rev. A* **50**, 3492 (1994).
64. M. Hillery and M. S. Zubairy, *Phys. Rev. A* **29**, 1275 (1984).
65. D. D. Crouch and S. L. Braunstein, *Phys. Rev. A* **38**, 4696 (1988).
66. P. Kinsler, M. Fernée, and P. D. Drummond, *Phys. Rev. A* **48**, 3310 (1993).
67. S. L. Braunstein and C. M. Caves, *Phys. Rev. A* **42**, 4115 (1990).